BIPV/T facades – A new opportunity for integrated collector-storage solar water heaters? Part 2

BIPV/T facades – a new opportunity for Integrated Collector-Storage Solar Water Heaters?

Part 2: Physical realisation and laboratory testing

Adrian Pugsley[(a)] (a.pugsley@ulster.ac.uk, +44(0)28 90366264 (corresponding author)
Aggelos Zacharopoulos[(a)] (a.zacharopoulos@ulster.ac.uk) +44(0)28 90368227
Jayanta Deb Mondol[(a)] (jd.mondol@ulster.ac.uk) +44(0)28 90368037
Mervyn Smyth[(a, b)] (m.smyth1@ulster.ac.uk) +44(0)28 90368119

(a) Centre for Sustainable Technologies (www.cst.ulster.ac.uk), School of the Built Environment, Ulster University, Newtownabbey, BT37 0QB, Northern Ireland, UK

(b) SolaForm Ltd (www.solaform.com) c/o Ulster University, Newtownabbey, BT37 0QB, Northern Ireland, UK

Keywords

Integrated Collector-Storage Solar Water Heaters (ICSSWH); Photovoltaic-Thermal (PV/T); thermal diode; building facade; solar collector; heat removal factor

Highlights

- Two-part study proposing an alternative approach to realising BIPV/T facades
- Part 1 reviews theory & potential, Part 2 describes prototype realisation & testing
- Integrated Collector-Storage Solar Water Heater (ICSSWH) element reduces overheating
- Planar Liquid-Vapour Thermal Diode (PLVTD) element reduces overnight heat losses
- Experimental results offer BIPV-PLVTD-ICSSWH benchmarks & validate theoretical model

Abstract

Building Integrated Photovoltaic Thermal (BIPV/T) systems which generate electricity and heat simultaneously are promising solutions for Net Zero Energy Buildings (NZEB). Despite BIPV/T offering clear energetic and space saving advantages compared to separate PV and solar thermal, overheating problems occur when no thermal demand exists, resulting in reduced yields, stagnation damage, and excessive fluid flow pressures. This two-part study examines an alternative approach combining BIPV, Planar Liquid-Vapour Thermal Diodes (PLVTD) and Integrated Collector-Storage Solar Water Heaters (ICSSWH) to achieve BIPV/T functionality and retain heat overnight to minimises parasitic demands and reduce overheating. The introductory paper (Part 1 of 2) established novelty and rationale for BIPV-PLVTD-ICSSWH concepts, reviewed

state-of-the-art and performance benchmarks, and used theoretical modelling to predict behaviour from key design and operational parameters. This paper (Part 2 of 2) describes prototype realisation and multi-day solar simulator laboratory thermal and photovoltaic testing for covered and uncovered variants exposed to different irradiance levels. Measured solar thermal efficiencies with and without transparent covers were $\eta_{T,col}$ = 60% and 58% respectively under zero heat loss conditions whilst overnight heat loss coefficients were $U_{r,sys}A_{sys}/u$ = 23.0 and 25.4 $W \cdot m^{-3}K^{-1}$ respectively, showing good agreement with theoretical predictions. Photovoltaic performance reduced with increasing absorber temperature as expected, although maximum power point efficiencies ($\eta_{E,mpp}$ = 11.4% at $T_1 \approx 25°C$ and 5.6% at $T_1 \approx 89°C$, without cover) were lower than expected owing to partial delamination and PV cell damage. The work demonstrates practical operation of a vertical BIPV-PLVTD-ICSSWH, identifies key areas for design development, and highlights benefits of application in NZEB facades.

Graphical abstract

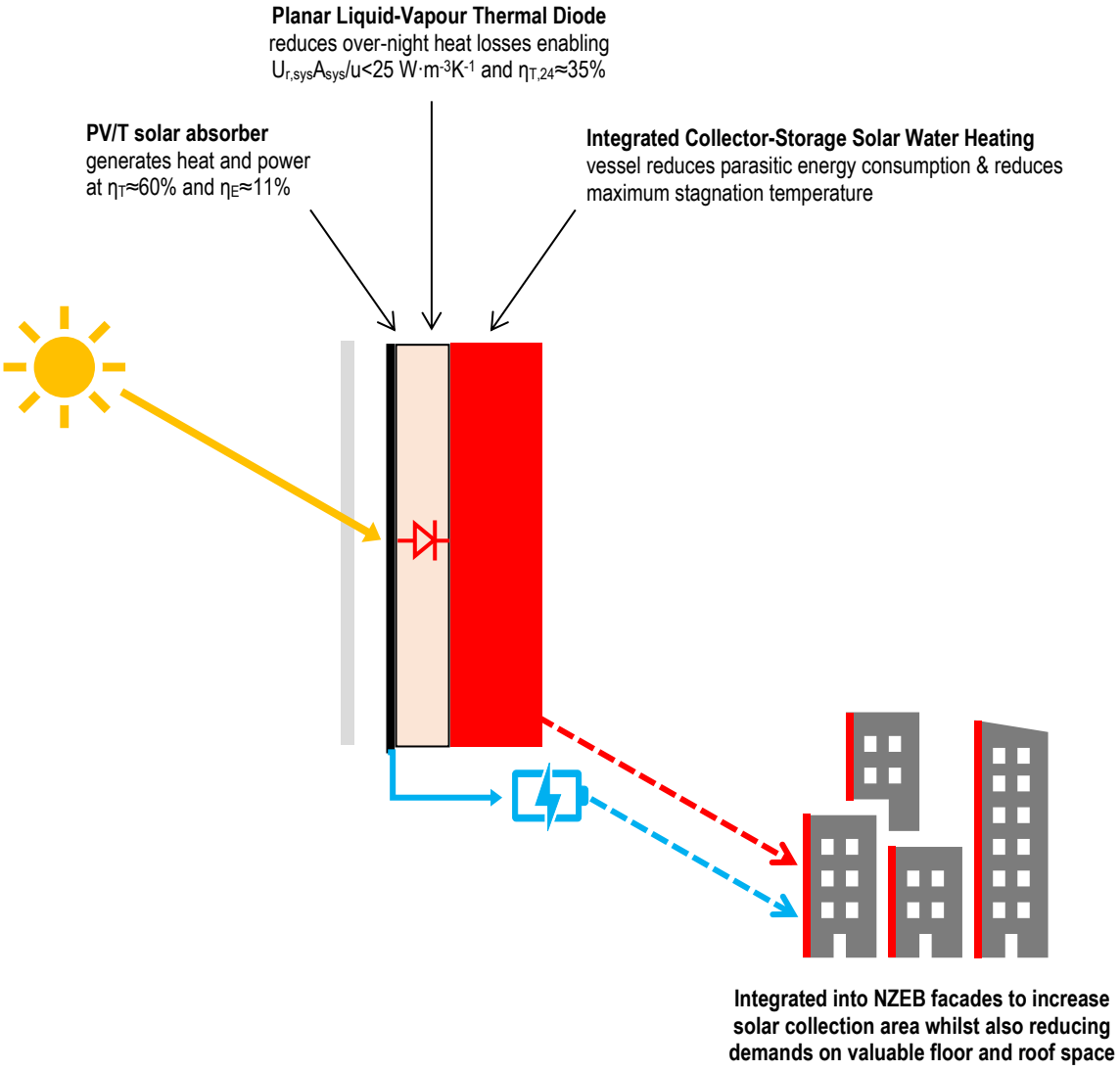

1 Introduction

Net Zero Energy Buildings (NZEB) and Near Zero Energy Buildings (nZEB) are increasingly being designed with Building Integrated Photovoltaics (BIPV) to generate electricity and Building Integrated Solar Thermal Systems (BISTS) to supply domestic hot water and contribute towards space heating demands (COST, 2015; Good, 2015). Mismatches between energy demands and solar availability (instantaneously, diurnally and over inter-seasonal timescales) mean that thermal energy storage is an essential part of most BISTS and is crucial for achievement of a high solar fraction (Affolter et al., 2006; Drosou et al., 2014). Electrical energy storage is likewise crucial for high solar fraction BIPV systems (Kats and Seal, 2012; Sorgato et al., 2018; Belussi et al., 2019). Building Integrated Photovoltaic-Thermal (BIPV/T) façade systems combine solar electricity and thermal energy (hot air and/or water) generation into vertical elements of building envelopes to make efficient use of all available insolated surfaces (Zondag, 2008; Yang & Athienitis, 2016). This is important for NZEBs where there is a high ratio of energy demand to envelope surface area, and in particular to the case of tall buildings where roof space for solar collectors is inherently limited. The most common realisation of water-heating PV/T collectors is to bond a conventional PV module to the absorber of a conventional sheet-and-tube flat solar water heater (Dupeyrat et al., 2011; Calise et al., 2016) or other planar heat removal device (Kazemian et al., 2018; Fayaz et al., 2019). Despite offering clear energetic advantages when suitable thermal demands exist, PV/T collectors suffer similar stagnation and overheating problems as closed-back BIPV systems (ie reduced electrical yields and eventual delamination damage) and conventional solar flat plate solar water heaters (ie over-pressurisation, denaturing of heat transfer fluids, damage to selective coatings, melting of polymeric components) when no thermal demands exist (Dupeyrat et al., 2011; Hasanuzzaman et al., 2016; Lazzarin and Noro, 2019). Stagnation overheating can be avoided by ensuring continuous fluid flows on hot sunny days but the corresponding parasitic energy requirements (eg for pumps and/or heat rejection fans) would have potential to far exceed the corresponding modest gains in electrical yields and the ancillary equipment needed (large thermal stores and/or heat rejectors) occupies valuable floor space.

Integrated Collector-Storage Solar Water Heaters (ICSSWH) are an alternative to conventional flat plate or evacuated tube collector solar water heating systems. Whilst

ICSSWH systems suffer significant overnight heat losses (eg unavailability of stored heat for morning bathing etc) they offer a number of advantages in respect of cost, space, and inherent passive protection from overheating. Recent studies by Pugsley et al. (2016, 2017, 2019, 2020) proposed the use of Planar Liquid-Vapour Thermal Diodes (PLVTD) to reduce problems of overnight heat loss in flat-form ICSSWH collectors. Studies by Krauter (2004) and Ziapour et al. (2014) examined the performance (respectively through experimental and simulation work) of novel PV-ICSSWH devices and identified a dearth of published work on similar concepts. Development of the novel BIPV-PLVTD-ICSSWH approach proposed in this two-part study has the potential to overcome key problems associated with the individual technologies (namely, BIPV/T overheating during stagnation, and ICSSWH overnight heat losses) and to realise new synergies. An exploded diagram illustrating the component parts of a BIPV-PLVTD-ICSSHW collector is shown in Figure 1. The fundamental principles of PV/T, ICSSWH and PLVTD concepts underpinning this study were reviewed in our introductory paper (Part 1 of 2) which also established state-of-the-art performance benchmarks and examined the expected energetic behaviour using a theoretical heat transfer model. The present paper (Part 2 of 2) concludes the study on this novel approach to BIPV/T by describing the realisation of a BIPV-PLVTD-ICSSWH prototype and presenting results of multi-day solar simulator laboratory tests for covered and uncovered variants exposed to different irradiance levels. This paper presents the measured temperatures, solar thermal collection, photovoltaic generation, and overnight heat retention efficiencies to establish performance benchmarks for the first ever BIPV-PLVTD-ICSSWH prototype, and compares these against theoretical modelling predictions in order to validate the model and identify key aspects of the design which can be improved. The key benefits and challenges associated with practical implementation of BIPV-PLVTD-ICSSWH concepts to support realisation of NZEBs as part of global decarbonisation efforts to tackle the climate crisis is also reviewed, with specific focus on building façade and heat pump system integration.

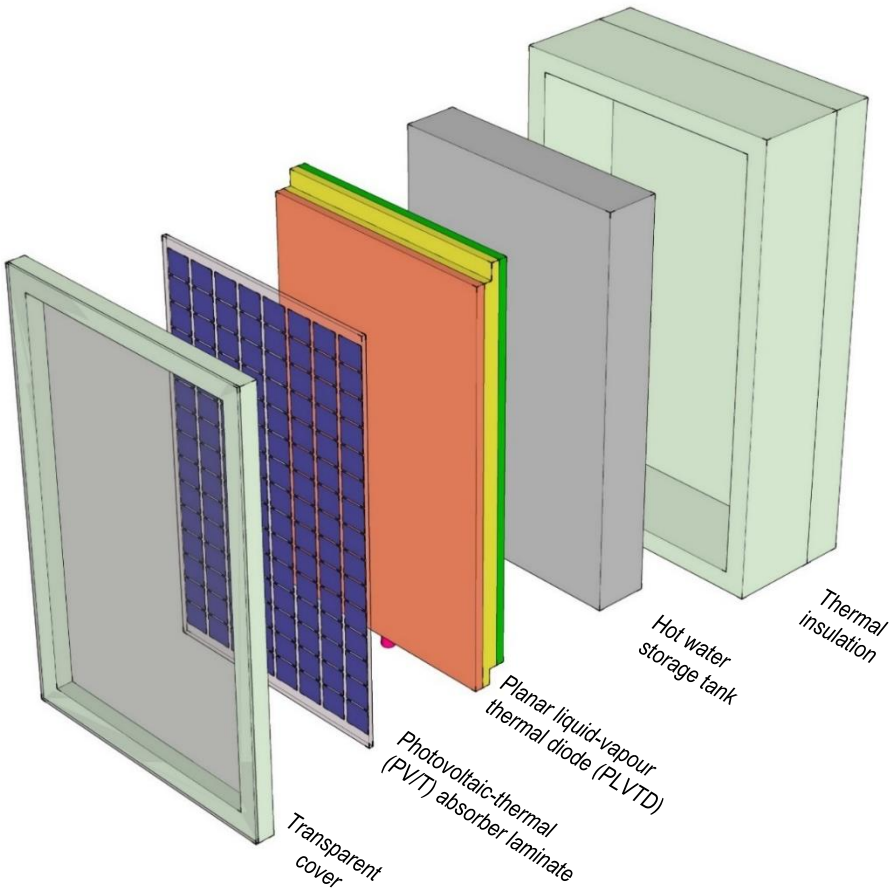

Figure 1: Key components of the BIPV-PLVTD-ICSSWH concept

2 Operating principles and performance benchmarks

The fundamental physical arrangement of the BIPV-PLVTD-ICSSWH device proposed in Figure 1 can be represented by the lumped parameter model shown in Figure 2. The model describes how the input solar irradiance (G) passes through transparent cover layers (optical transmissivity τ) before being absorbed by the PV cells (solar absorptivity α and temperature T_0) which convert the incident solar flux into thermal energy and electrical energy. The thermal power is either lost (q_{0a}) to the ambient environment (at temperature T_a) or transferred (q_{03}) through the thermal diode via the evaporator (at temperature T_1) and condenser (at temperature T_2) to heat the water storage tank (at temperature T_3) where it becomes available for delivery to thermal loads (q_T). Some of the solar heat gained by the tank is lost through the insulated tank sidewalls and back plate (q_{3ia}). Thermal diode heat losses (q_{4ia}) from the insulated PLVTD sidewalls (at temperature T_4) are neglected as these are small by comparison. Absorber heat losses (q_{0a}) pass through the absorber laminate (from the cells at temperature T_0 to the front surface at T_5) and airgap to the transparent cover (at

temperature T_6) and eventually to the ambient. The amount of electrical power produced by the PV cell array ($q_E=I_{PV}\cdot V_P$) is dependent upon the irradiance; the pump and load electrical resistances; and the PV cell array electrical characteristics, which are themselves dependent upon the PV cell material properties and temperature. Some of the electrical power generated by the PV is delivered to a small pump (q_P) which distributes a working fluid film to wet the PLVTD evaporator and the remainder (q_{load}) is available to serve applied electrical loads. Further details of the theoretical model together with corresponding mathematical expressions and scenario simulations are presented in a separate paper (Part 1 of 2) which serves as the introduction to this two-part study.

Thermal power gained by an ICSSWH during solar collection periods is usually determined using either quasi steady-state or whole-day testing based upon the rate of temperature rise of the stored thermal mass ($q_T = M\cdot c_p\cdot \Delta T_3/t_{col}$) where q_T is the heat gain, $M\cdot c_p$ is the mass and specific heat capacity product of the thermal store, and ΔT_3 is the rise in thermal store temperature during a collection period of duration t_{col}. Loss of stored heat overnight is likewise determined in a similar manner with reference to the heat retention period duration t_{ret}. Equations 1 to 3 define the solar thermal collection efficiency ($\eta_{T,col}$), heat retention efficiency ($\eta_{T,ret}$), and heat loss coefficient ($U_{r,sys}A_{sys}$). Collection efficiencies are evaluated with reference to total insolation (H) which is the product of the irradiance (G) incident on the collector aperture (area A_1) during the collection period. Retention efficiencies are evaluated with reference to the amount of heat contained within the thermal store at the start of the retention period (assumed to commence at the end of the preceding collection period) and are normalised in relation to ambient temperatures at the end of the collection period ($T_{a[t_{col}]}$) and averaged throughout the retention period ($\tilde{T}_{a[t_{ret}]}$). Collection performance is influenced by the solar thermal condition (Equation 4) such that the highest efficiencies occur when the stored water temperature is close to the ambient temperature (zero heat loss when N=0 because $T_3=T_a$) and efficiency reduces with increasing ΔT_{3a}, especially when the irradiance is low. The introductory paper of this study (Part 1 of 2) established $\eta_{T,col}\approx 60\%$ at $N\approx 0.035$ $m^2K\cdot W^{-1}$ as a state-of-the-art benchmark for ICSSWH collection efficiency and also established benchmark specific heat loss coefficients of $U_{r,sys}A_{sys}/A_1\approx 1$ $W\cdot m^{-2}K^{-1}$ and $U_{r,sys}A_{sys}/u\approx 10$ $W\cdot m^{-3}\cdot K^{-1}$ at $\Delta T_{3a}\approx 25°C$, where u is the water storage tank volume. Heat could feasibly be drawn

to serve thermal load demands at any time of day (eg morning or evening bathing, space heating at night, etc) hence Equation 5 describes the diurnal thermal efficiency ($\eta_{T,24}$) which is a composite of the collection and retention efficiencies. Provided that t_{col} and t_{ret} cover a contiguous 24 hour period then $\eta_{T,24}=1$ describes the hypothetical case where all available solar energy is collected and then retained without loss, whereas $\eta_{T,24}=0$ would occur if no heat was collected or all collected heat was lost.

Photovoltaic cells and modules are commonly characterized with reference to Standard Test Conditions (STC at G=1000 W/m^2 irradiance with spectrum AM1.5 and T_0=25°C cell temperature) using performance metrics derived from current-voltage curves. Performance of PV/T collectors commonly deviates significantly from that occurring under STC because cells are operated at elevated temperatures in order to deliver useful heat. The cell temperature (T_0) is determined by the absorber temperature (T_1) which in turn is determined by a combination of ambient temperature (T_a) and fluid delivery temperature (T_3). The inclusion of transparent covers over the absorber reduces the influence of T_a to enable high T_3 and/or operation in cold and windy climates but unfortunately covers also introduce optical losses which reduce the level of irradiance incident on the PV cells. Key performance metrics for PV elements (defined in Equations 6 to 9) include short circuit current (I_{sc}), open circuit voltage (V_{oc}), electrical power delivered at the maximum power point ($q_{E,mpp}$), fill factor (FF), voltage-temperature coefficient ($K_{V:T}$), current-temperature coefficient ($K_{I:T}$) and voltage-irradiance coefficient ($K_{V:G}$).

$$\eta_{T,col} = \frac{Energy\ in\ store\ at\ t{=}t_{col}}{Energy\ incident\ from\ t{=}t_0\ to\ t{=}t_{col}} = \frac{M{\cdot}c_p\left(T_{3[t=t_{col}]} - T_{3[t=t_0]}\right)}{H{\cdot}A_1} \qquad \text{Equation 1}$$

$$\eta_{T,ret} = \frac{Retained\ energy\ in\ store\ at\ t{=}t_{col}{+}t_{ret}}{Energy\ in\ store\ at\ t{=}t_{col}} = \frac{M{\cdot}c_p\left(T_{3[t=t_{col}+t_{ret}]} - \tilde{T}_{a[t_{ret}]}\right)}{M{\cdot}c_p\left(T_{3[t=t_{col}]} - T_{a[t=t_{col}]}\right)} \qquad \text{Equation 2}$$

$$U_{r,sys}A_{sys} = \frac{M{\cdot}c_p}{t_{ret}}\ln\left(\frac{1}{\eta_{T,ret}}\right) \qquad \text{Equation 3}$$

$$N = \frac{\tilde{T}_3 - \tilde{T}_a}{t_{col}\int_{t=0}^{t=t_{col}} G} \qquad \text{Equation 4}$$

$$\eta_{T,24} = \eta_{T,col} \cdot \eta_{T,ret} \qquad \text{Equation 5}$$

$$q_{E,mpp} = I_{mpp} \cdot V_{mpp} = FF \cdot I_{sc} \cdot V_{oc}$$ Equation 6

$$K_{V:T} = \frac{V_{oc,T_0} - V_{oc,STC}}{V_{oc,STC}\,(T_0 - 25)}$$ Equation 7

$$K_{I:T} = \frac{I_{sc,T_0} - I_{sc,STC}}{I_{sc,STC}\,(T_0 - 25)}$$ Equation 8

$$K_{V:G} = \frac{V_{oc,G}}{V_{oc,STC}}$$ Equation 9

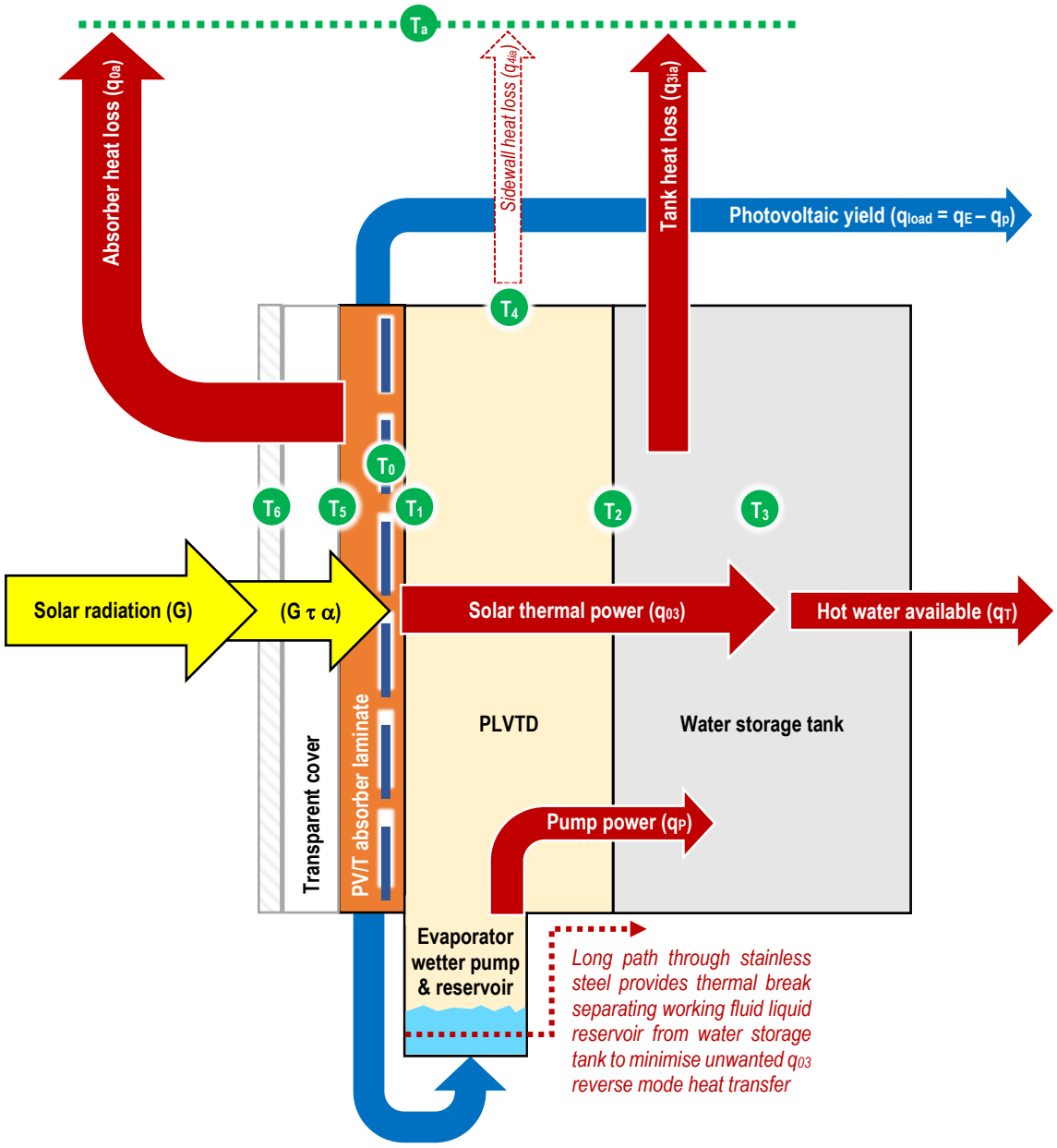

192

193

G	Incident solar radiation flux	Gτα	Absorbed solar radiation
T_a	Ambient environmental temperature	q_{03}	Thermal power transferred from the absorber to the water storage tank through the thermal diode
T_0	Photovoltaic cell temperature	q_T	Net rate of heat gained by the stored water bulk
T_1	Temperature of absorber laminate substrate and PLVTD evaporator plate	q_{0a}	Heat loss from PV cells
T_2	Temperature of condenser plate and tank mantle	q_{3ia}	Heat loss from the back and sides of the water storage tank not covered by the thermal diode
T_3	Temperature of water bulk stored in the tank	q_{4ia}	Heat loss from PLVTD sidewalls
T_4	Thermal diode sidewall temperature	q_E	Electrical power yielded from PV
T_5	Absorber laminate surface temperature	q_P	Electrical power consumed by the evaporator wetter pump which is then all converted to heat
T_6	Transparent cover temperature	q_{load}	Electrical power delivered to load

194 ***Figure 2: Lumped parameter model of a BIPV-PLVTD-ICSSWH***

3 Experimental work

3.1 Design and realisation of a prototype

The design of a laboratory prototype BIPV-PLVTD-ICSSWH collector was developed with due consideration for constraints imposed by building and façade integration (see Section 4). A prototype with z=1400 mm high by y=700 mm wide absorber and 100L capacity water storage tank was fabricated, consisting of the key components illustrated on Figure 1 with properties as detailed in Table 1:

1) Removable transparent acrylic cover set over a sealed air-filled cavity in order to insulate against solar absorber heat losses.

2) Solar PV/T absorber formed of 120 quartered mc-si PV cell pieces (78x78mm) covered by transparent acrylic plates bonded to the matt black painted PLVTD evaporator plate using transparent silicone resin. The PV cell pieces were arranged as 15 separate strings (each forming a row of 8 cell pieces, as shown on Figure 3) and bonded to, and electrically isolated from, the stainless steel substrate by 5 small pieces of 1mm thick self-adhesive polyurethane foam. The PV cells were electrically interconnected in a series-parallel configuration on 5 buses (labelled A to E on Figure 3) to produce $V_{oc} \approx 24$ V and sufficient current ($I_p \approx 0.5$ A) to drive the evaporator wetter pump.

3) Stainless steel PLVTD constructed of 0.9mm plates and sidewalls with 200 cylindrical tubular internal support struts. A novel cross-sectional shape was developed to enable integration of the working fluid reservoir without causing a liquid thermal bridge (see Figures 2&4). The evaporator wetting system consisted of a small manifold-mount centrifugal pump fitted to the reservoir base with a stainless steel pipe supplying fluid to a linear distribution nozzle at the head of the evaporator plate to create a falling film. Refer to Pugsley (2017) and Pugsley et al. (2020) for further details concerning PLVTD design attributes.

4) Flat profile open-top water storage tank formed of stainless steel sheet folded into a 4-sided rectangular box shape, welded to the PLVTD condenser plate, and insulated externally on all sides (including lid) with polystyrene foam.

Prototype fabrication commenced with the metalwork fabrication (see Pugsley, 2017; Pugsley et al., 2020 for more details) according to the arrangement shown on Figure 4. After repairing minor envelope vacuum leaks at welded joints, the PLVTD enclosure was evacuated to 0.01 kPa, which removed non-condensable gases and enabled injection of 0.9kg working fluid through an arrangement of valves. The prototype was

then mounted on a frame before fitting thermocouples and insulation. The PV cells were cut to size using Ulster University's specialist high velocity ceramic disc cutting machine and soldered to apply tinned copper electrical tabbing. Finally, the absorber surface was painted, the PV cells strings were assembled, and mounted, encapsulating resin was cast in place, and power cables were connected as illustrated on Figures 3 & 5. Unfortunately, despite care being taken to protect the PV, damage was sustained to several cells in the process of fixing and casting them in place.

Table 1: Key properties of the BIPV-PLVTD-ICSSWH prototype

Quantity	Value	Unit	Basis
Volume of water in storage tank (u)	0.1	m^3	Typical tank size reported in literature* on ICSSWH systems
Aperture and absorber area (A_1)	1	m^2	Typical absorber size reported in literature* on ICSSWH systems
PV cell coverage of absorber area (A_0)	0.75	m^2	15 strings, each formed of 8 quarter-cell pieces (78x78mm)
Absorber laminate thickness (x_{15})	5	mm	Absorber laminate consisted of PV cells cast in transparent crystal-clear silicone resin (nominal 2mm overall thickness). Resin was bonded to stainless steel substrate and faced with 3mm transparent acrylic sheet
Removeable transparent cover thickness (x_{56})	33	mm	Comprising of 3mm transparent acrylic sheet mounted on a polystyrene foam frame to form 30mm air gap between absorber and cover
Depth of PLVTD (x_{12})	70	mm	Dimension as discussed by Pugsley et al. (2020)
Depth of tank (x_3)	100	mm	Tank volume divided by absorber area
Standard power output of PV cell (q_{STC})	4.24	W	156x156mm pseudo square mc-si M-2BB solar PV cell (Bosch, 2010)

*The reader is directed to the literature review presented in our study introduction paper (Part 1 of 2)

3.2 Experimental method

The aim of the experimental work was to investigate the behaviour of the whole BIPV-PLVTD-ICSSWH prototype collector under representative operating conditions to validate expected behaviours predicted by the theoretical model in terms of solar thermal and photovoltaic collection efficiencies, overnight heat retention, and diurnal thermal efficiency. The thermal test experimental methodology largely follows the precedents set by Smyth et al. (2003, 2015, 2018 & 2019) and Muhumuza et al. (2019) whereby the prototype is exposed to constant simulated solar irradiance before being left to cool overnight. Most previously documented solar simulator tests on ICSSWH prototypes have covered a single 24h period whereas each test in the present work covered a 100h period corresponding to 4 consecutive days. Our preceding paper (Part 1 of 2) which introduces the present study sets out a table of insolation and average irradiance levels for three contrasting climate locations (Belfast, UK; Rome, Italy; Riyadh, Saudi Arabia) at different latitudes based on 22 years of extra-terrestrial solar radiation measurements and earth surface satellite imagery (NASA, 2019; Stackhouse et al., 2018). Equator-facing vertical surfaces such as building facades

(assuming no shading) in Rome receive H_{24}≈12 MJ/m^2 during both summertime and wintertime periods. Lower vertical plane insolation values typically occur in Riyadh during summer (H_{24}≈7 MJ/m^2 due to the acute incident angles associated with high solar altitudes) and also in Belfast (H_{24}≈9 MJ/m^2 in summer and H_{24}≈4 MJ/m^2 in winter owing to the predominantly cloudy local climate). Higher vertical plane insolation values are common in Riyadh during winter (H_{24}≈14 MJ/m^2) and at the spring and autumn equinoxes in Rome where H_{24}≈20 MJ/m^2) occurs on the sunniest days. In order to be representative of the stable mid-range insolation conditions in Rome and to account broadly for the typical minima and maxima, the following four separate 100h tests were undertaken:

1) Moderate daily insolation (H_{24}=13.2MJ/m^2) with a transparent cover.
2) Moderate daily insolation (H_{24}=13.2MJ/m^2) without a transparent cover.
3) Low daily insolation (H_{24}=8.0MJ/m^2) without transparent cover.
4) High daily insolation (H_{24}=18.8MJ/m^2) without transparent cover.

These daily insolation scenarios were simulated using 6h periods of exposure to columnated vertical plane irradiance of G=370, 610 and 870 W/m^2 (for low, moderate and high insolation scenarios respectively) incident on the prototype at an angle normal to the aperture plane. Irradiance was provided by the Ulster University solar simulator (Zacharopoulos et al., 2009; Arya et al., 2018) which consists of 35 metal halide lamps fitted with columnating lenses providing illumination uniformity of ±10% and an infrared filter to ensure realistic daylight spectrum similar to AM1.5.

The prototype was instrumented with 50 thermocouples (T-type, accuracy verified to to ±0.3°C) to measure temperatures of the various elements of the prototype (T_0, T_1, T_2, T_3, T_4, T_5, T_6 and T_a as per Figure 2) and to examine planar spatial variations. The majority of thermocouples were bonded to the metal body of the PLVTD or located within the water storage tank (see Figure 4) although some were attached to the rear of the PV cells (labelled according to cell number on Figure 3 as $T_{0\,(y,x)}$ where y = row number of string and x = cell column number) and embedded within the absorber laminate or fixed to the insulation and transparent cover elements (see Figures 3 & 6). Temperature readings were made using a datalogger (Delta-T DL2e) set to record every 5 minutes.

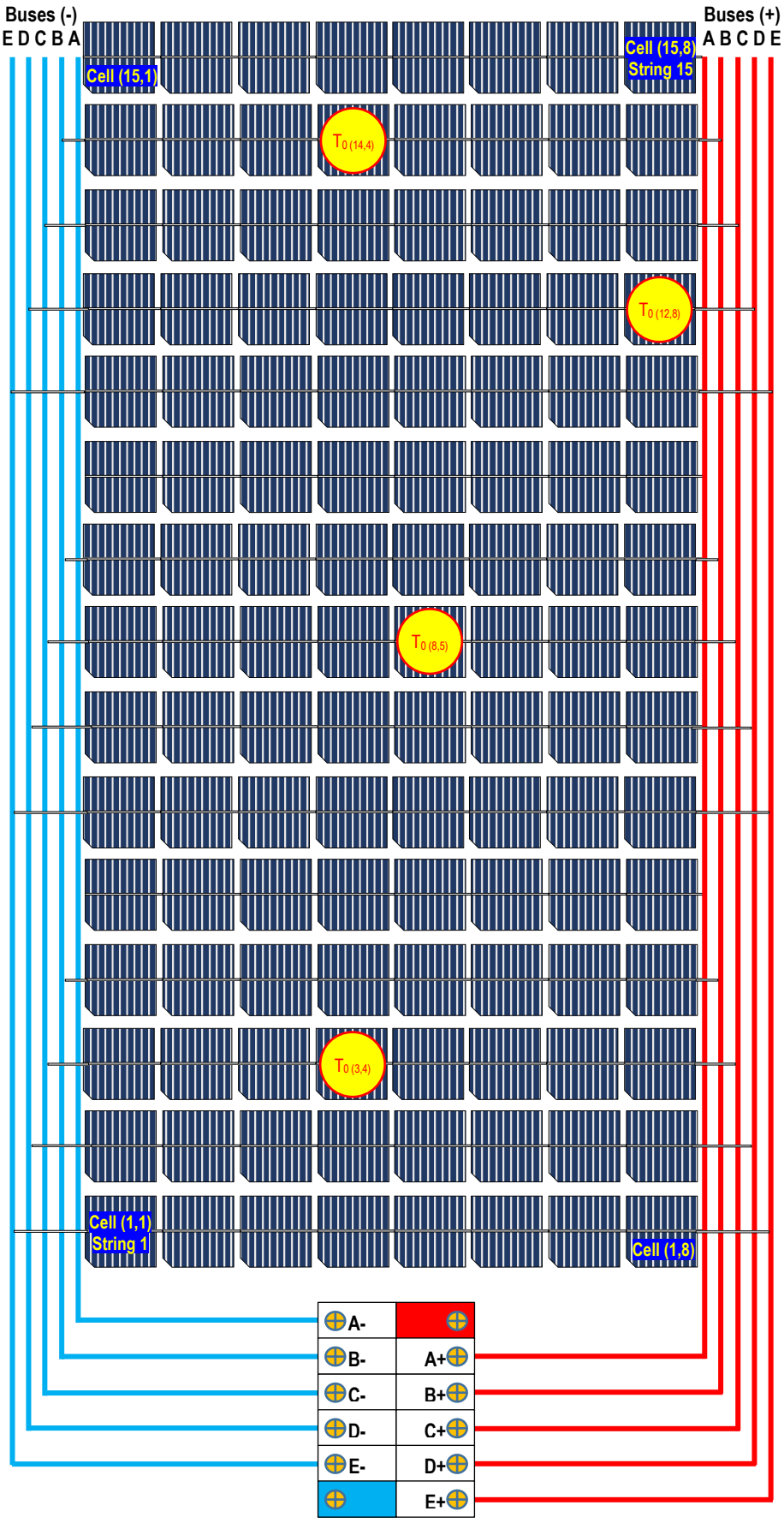

PV cell temperature measurement locations are denoted by $T_{0\,(y,x)}$ where y = row number of string and x = cell column number

Figure 3: Photovoltaic cell layout, series parallel wiring arrangement, and temperature measurement locations

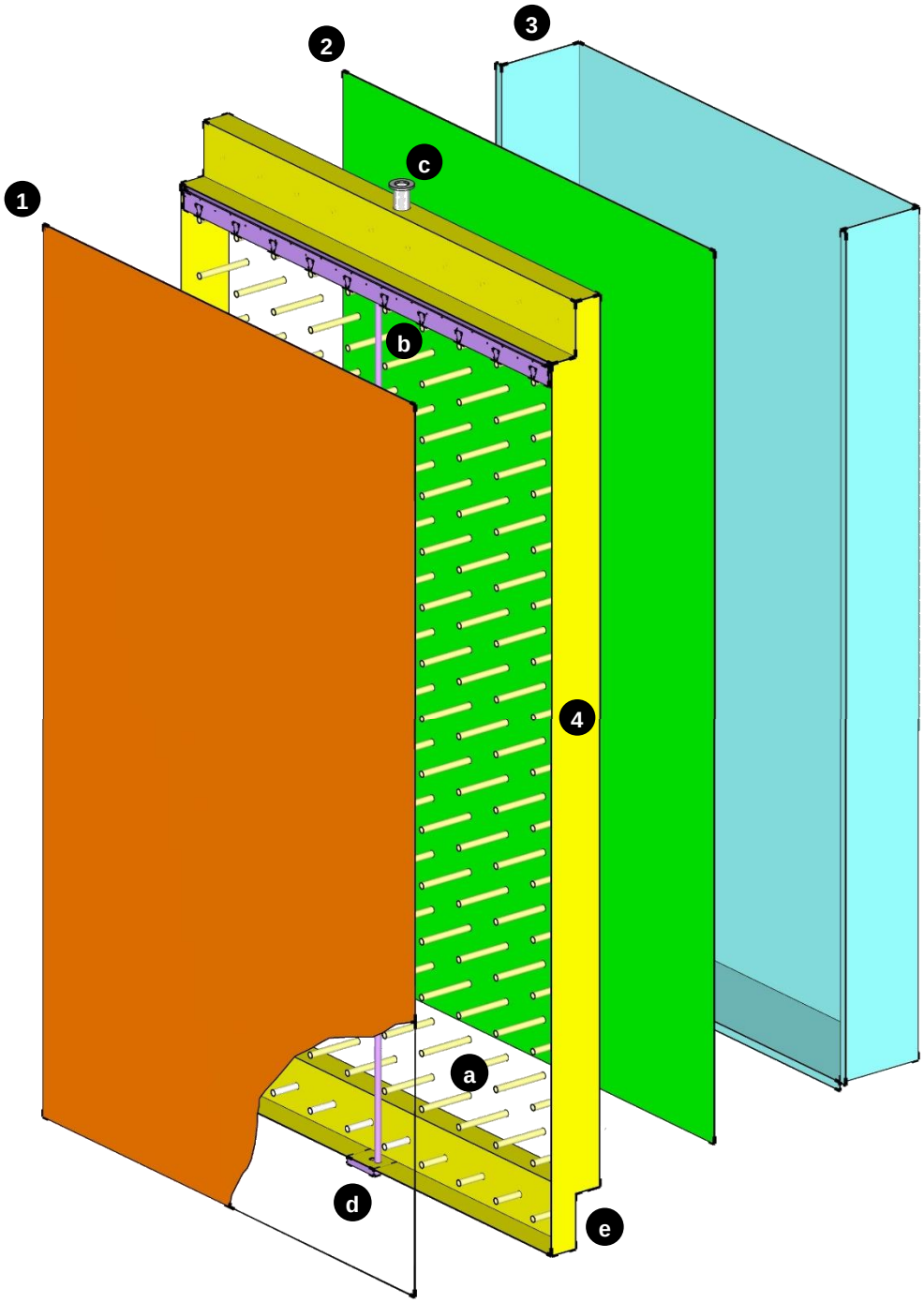

1) Absorber-Evaporator plate (12 thermocouples bonded to front surface to measure temperature T_1)
2) Condenser-tank plate (12 thermocouples bonded to rear surface to measure temperature T_2)
3) Water storage tank back, sides and base (5 submerged thermocouples measuring T_3)
4) Sidewalls forming the top, bottom and sides of the PLVTD envelope (5 thermocouples bonded to measure temperature T_4)
a) Array of tubular struts forming internal structure
b) Evaporator wetter distributer and diffuser nozzle
c) Spigot for vacuum pump connection and working fluid injection
d) Evaporator wetter pump mounting plate
e) Working fluid reservoir with thermal break separating from condenser plate

291

292 ***Figure 4: Exploded view of the PLVTD and water tank***

293 ***Figure 5: Photos showing PV/T absorber fabrication: All process stages (Top); Bare PV cells & cables (Left) Complete prototype (Right)***
294

The storage tank temperature (T_3) changes with time (t) and was used to calculate the instantaneous thermal power (q_3) delivered to or lost from the tank based on the relationship $q_3 = M \cdot c_p \cdot \Delta T_3 / t_{col}$. Initial tests were undertaken to determine thermal conductance of the insulated water storage tank and PLVTD sidewalls by covering the evaporator plate with 300mm of insulation, filling the tank with water at 70°C, and measuring the time taken to cool to T_a=23°C room temperature. Measurement results suggested residual heat loss of U_{3a}=1.1 $W \cdot m^{-2}K^{-1}$ over an area of A_{3ia}=2.3 m^2 decreasing with time to U_{3a}=0.6 $W \cdot m^{-2}K^{-1}$ as the tank temperature reduced towards ambient. Having quantified residual heat losses, the instantaneous heat fluxes through the absorber and thermal diode (q_{03}/A_1) and lost from absorber to ambient (q_{0a}/A_1) could be calculated with reference to the energy balance model (refer to our study introduction paper, Part 1 of 2). Tests were undertaken with the PV elements coupled to an electrical load throughout (load resistance was adjusted periodically to ensure maximum power point operation) but without any thermal load (no water draw-offs, to simulate multi-day stagnation behaviour). The electrical load was temporarily disconnected every 2 hours during each collection period (for about 5 minutes on each occasion) to permit sampling of the PV module current-voltage characteristics using a Daystar DS1000 curve tracer which automatically sweeps the load condition from I_{sc} to V_{oc} through the maximum power point operating condition ($q_{E,mpp}$). Supplementary measurement equipment included a calibrated pyranometer (Kipp & Zonen CM4) to measure irradiance levels; two Digital Multimeters (Amprobe AM-510-EUR) to monitor photovoltaic currents and voltages and measure load resistance; an Infrared Thermometer (Fluke 561) and a Thermal Imaging Camera (Testo 875-1i) to measure absorber surafce temperatures. The experimental procedure is detailed in full by Pugsley (2017) but is not repeated here for the sake of brevity.

3.3 Solar thermal collection and heat retention results

Temperature time histories with corresponding solar irradiances and absorber heat fluxes are shown on Figures 6 to 9 for each of the multi-day tests. Solar heat collection is apparent when the prototype is exposed to irradiance which causes the absorber-evaporator plate temperature (T_1) to rise and for heat flux ($150 < q_{03}/A_1 < 600$ $W \cdot m^{-2}$) to be transmitted to the condenser-tank plate (T_2) across the PLVTD temperature difference ($3 < \Delta T_{12} < 30$°C) causing a steady increase in water storage tank temperature from the starting condition $T_3 \approx T_a \approx 17$°C.

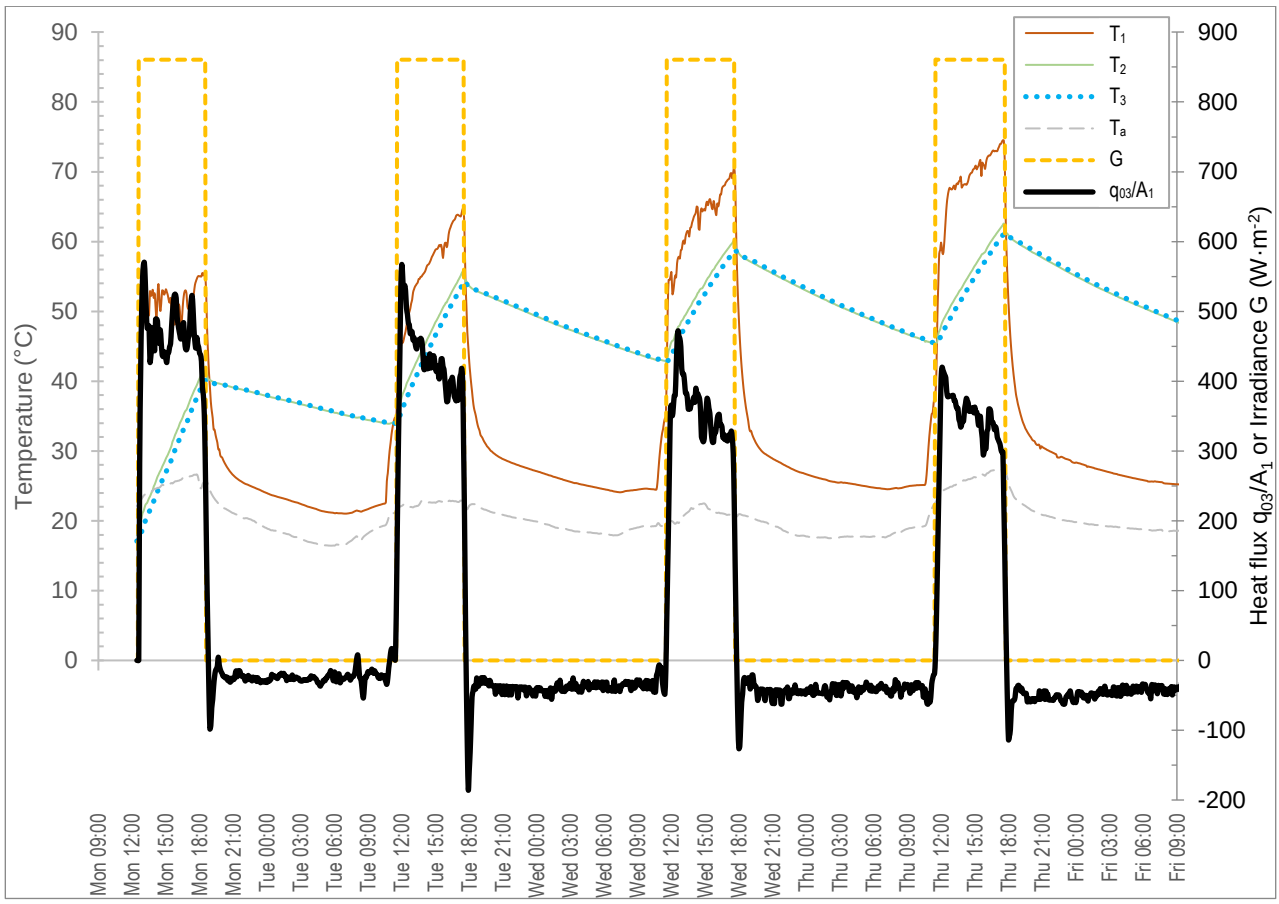

328
329 *Figure 6: Temperature and heat flux time history results for tests under high irradiance without absorber transparent cover*

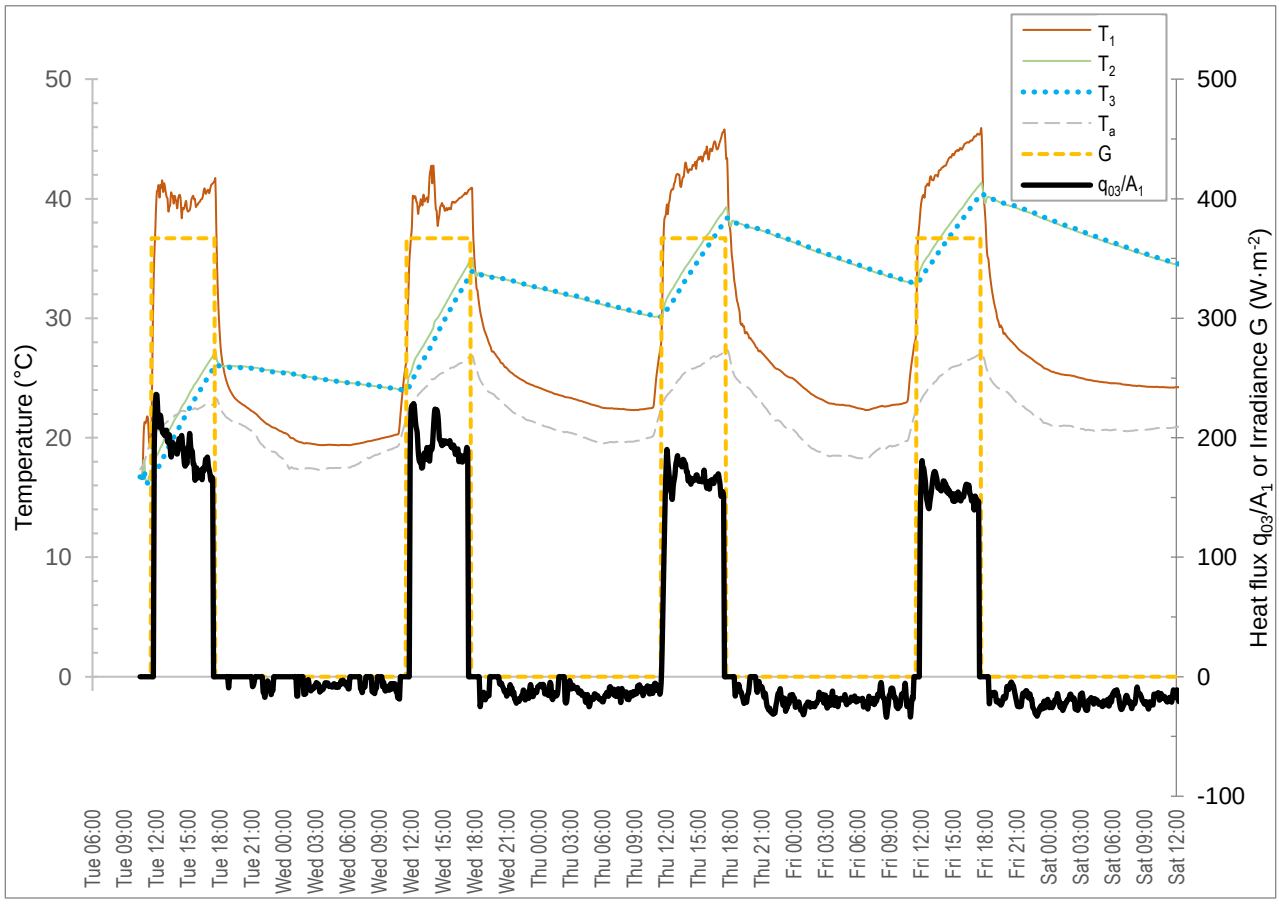

330
331 *Figure 7: Temperature and heat flux time history results for tests under low irradiance without absorber transparent cover*

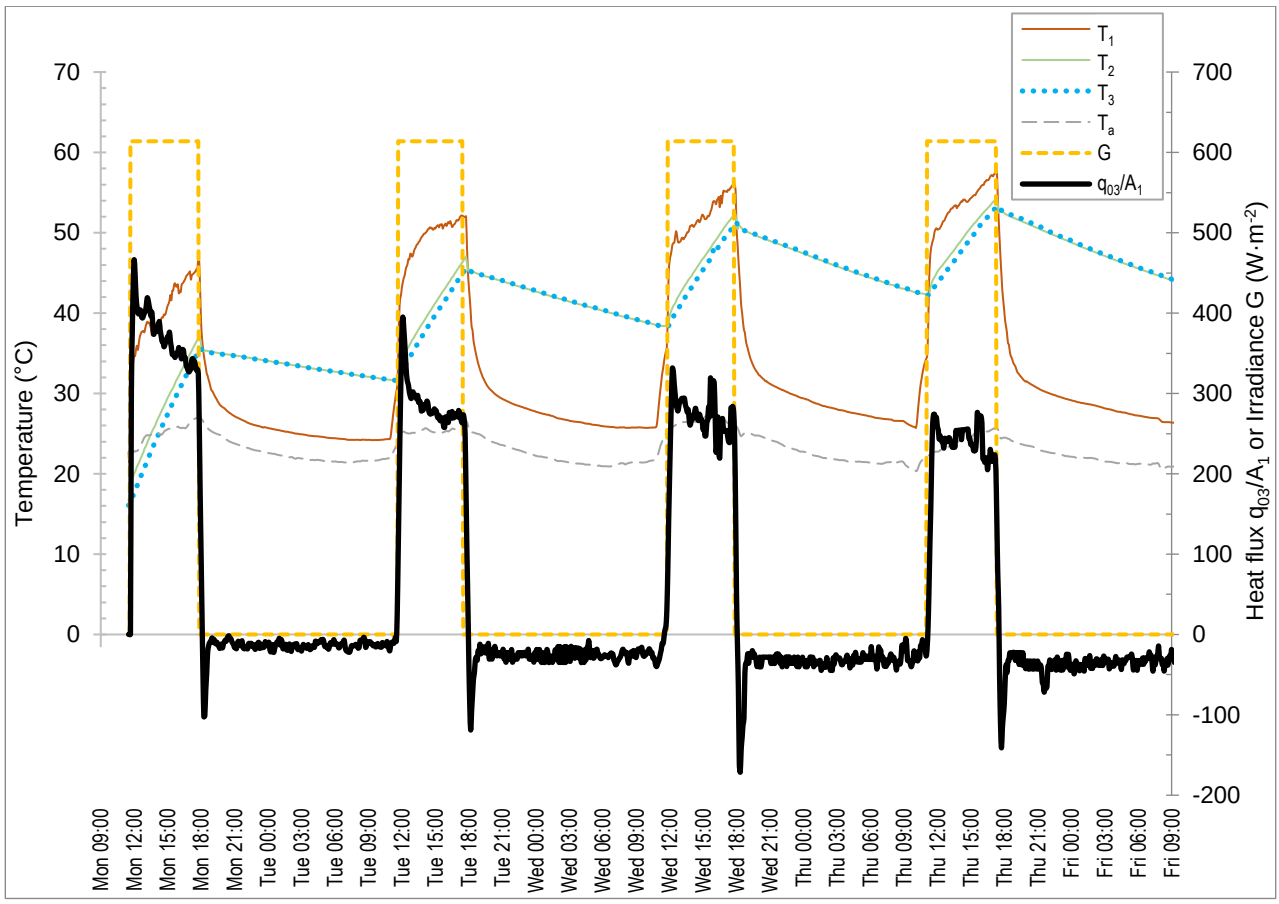

Figure 8: Temperature and heat flux time history results for tests under moderate irradiance without absorber transparent cover

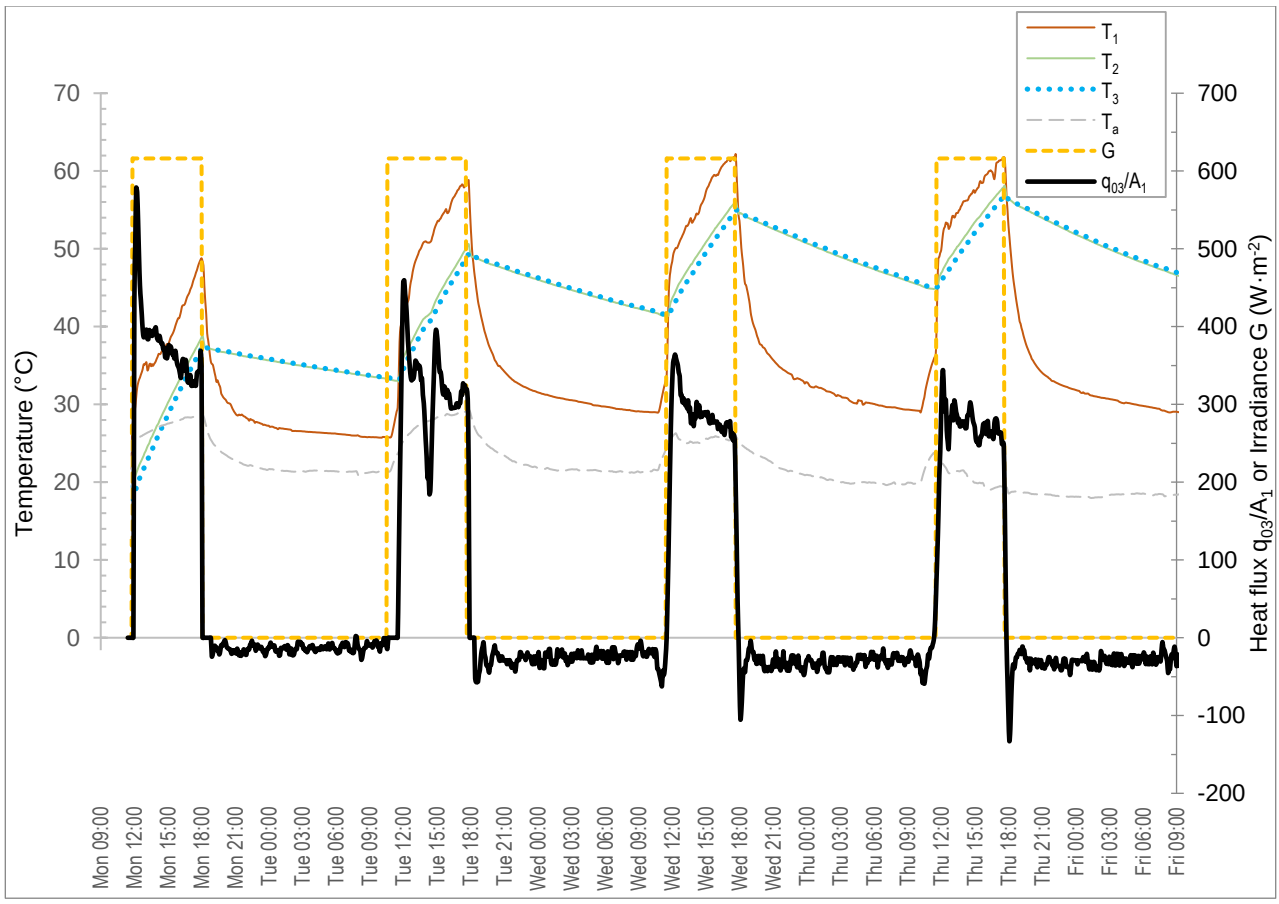

Figure 9: Temperature and heat flux time history results for tests under moderate irradiance with absorber transparent cover

Retention periods occur when irradiance ceases (G=0) causing absorber-evaporator plate temperatures to fall below those of the condenser-tank plate ($5<-\Delta T_{12}<25$°C) and for a steady heat loss flux ($15<-q_{03}/A_1<60$ W·m^{-2}) to develop causing a steady decrease in T_3. As discussed by Pugsley et al. (2020), the measured heat fluxes and temperature differences imply thermal diode conductances of $U_{f,12}\approx 38$W·m^{-2}K^{-1} in forward (collection) mode and $U_{r,12}=1.7$W·m^{-2}K^{-1} in reverse (retention) mode.

Water storage tank temperatures were observed to reach maxima of $T_3 = \tilde{T}_a + 34 =$ 61°C and $T_3 = \tilde{T}_a + 15 =$ 40°C by the end of Day 4 respectively for the high and low irradiance tests without transparent cover (see Figures 6 and 7). Day 4 maximum temperatures for the moderate irradiance tests without and with the transparent cover (see Figures 8 & 9) were respectively $T_3 = \tilde{T}_a + 29 =$ 53°C and $T_3 = \tilde{T}_a + 34.8 =$ 57°C which shows the beneficial effect of reducing absorber heat losses. These test results (obtained for $H_{24}=13.2$MJ/m^2 without wind) correspond reasonably closely to the theoretical modelling (refer to Figure 9 of our study introduction paper, Part 1 of 2) which predicted a Day 4 maximum temperature of $T_3 = \tilde{T}_a + 29.2 =$ 51.2°C for Variant B which is representative of a BIPV-PLVTD-ICSSWH with single transparent cover operating under average summertime conditions in Rome ($H_{24}=11.5$MJ/m^2 with 2m/s wind). This provides reasonable validation of the model when allowing for minor differences in insolation and the absence of wind during tests.

The measured instantaneous and daily solar thermal collection efficiencies are presented on Figure 10. Based on least-squares regression lines ($R^2>0.88$) fitted to the measured data, the zero-loss performances (N=0 m^{2}K·W^{-1}) of the bare absorber and single covered variants of the BIPV-PLVTD-ICSSWH collector are $\eta_T=58\%$ and 60% respectively. Measured performances at the benchmark solar thermal condition (N=0.035 m^{2}K·W^{-1}) are $\eta_T=40\%$ and 49% respectively, somewhat lower than the $\eta_T=60\%$ target for state-of-the-art ICSSWH collectors as expected, due to some of the incident energy (~10%) being converted to electricity rather than heat. Measured trends are in reasonable agreement with predicted performances which provides further model validation. Small discrepancies between modelled and measured results are primarily associated with the thermal diode conductance which was modelled as constant $U_{f,12} \approx 38$W·m^{-2}K^{-1} but varied in practice (95% of values varied in the range

±17 $W \cdot m^{-2}K^{-1}$ as reflected by the scatter in the measured data) owing to its temperature and heat flux dependence (refer to Pugsley et al., 2020). It should be noted that data on Figure 10 excludes transients during the first 30 minutes of each collection period when the rise in tank temperature occurs very much slower than the rise in absorber temperature owing to the lag introduced by the latent thermal mass associated with liquid-vapour phase change within the PLVTD. Apparent instantaneous solar thermal efficiencies during these transients were typically ~10% lower than the steady-state values.

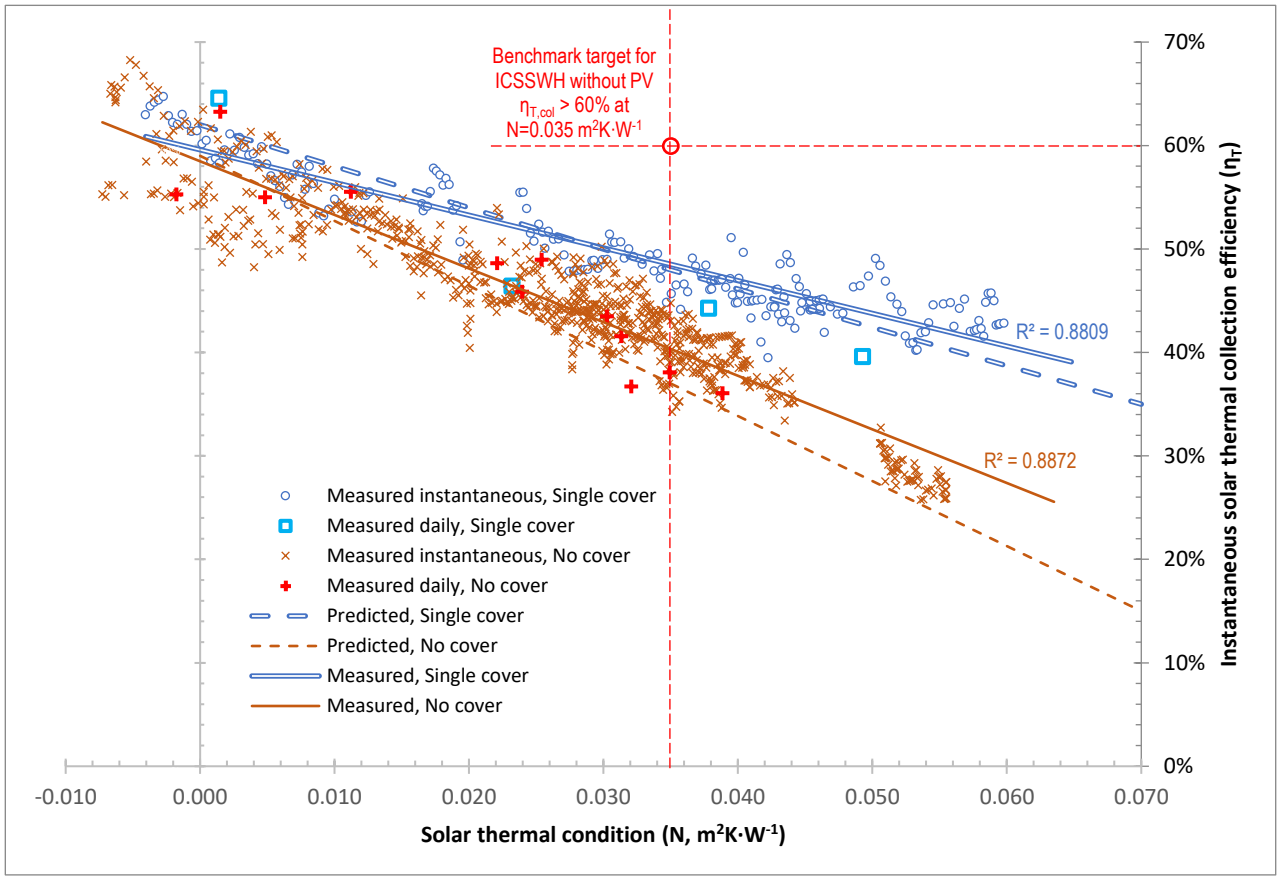

Figure 10: Solar thermal collection efficiency of BIPV-PLVTD-ICSSWH prototype with and without transparent cover

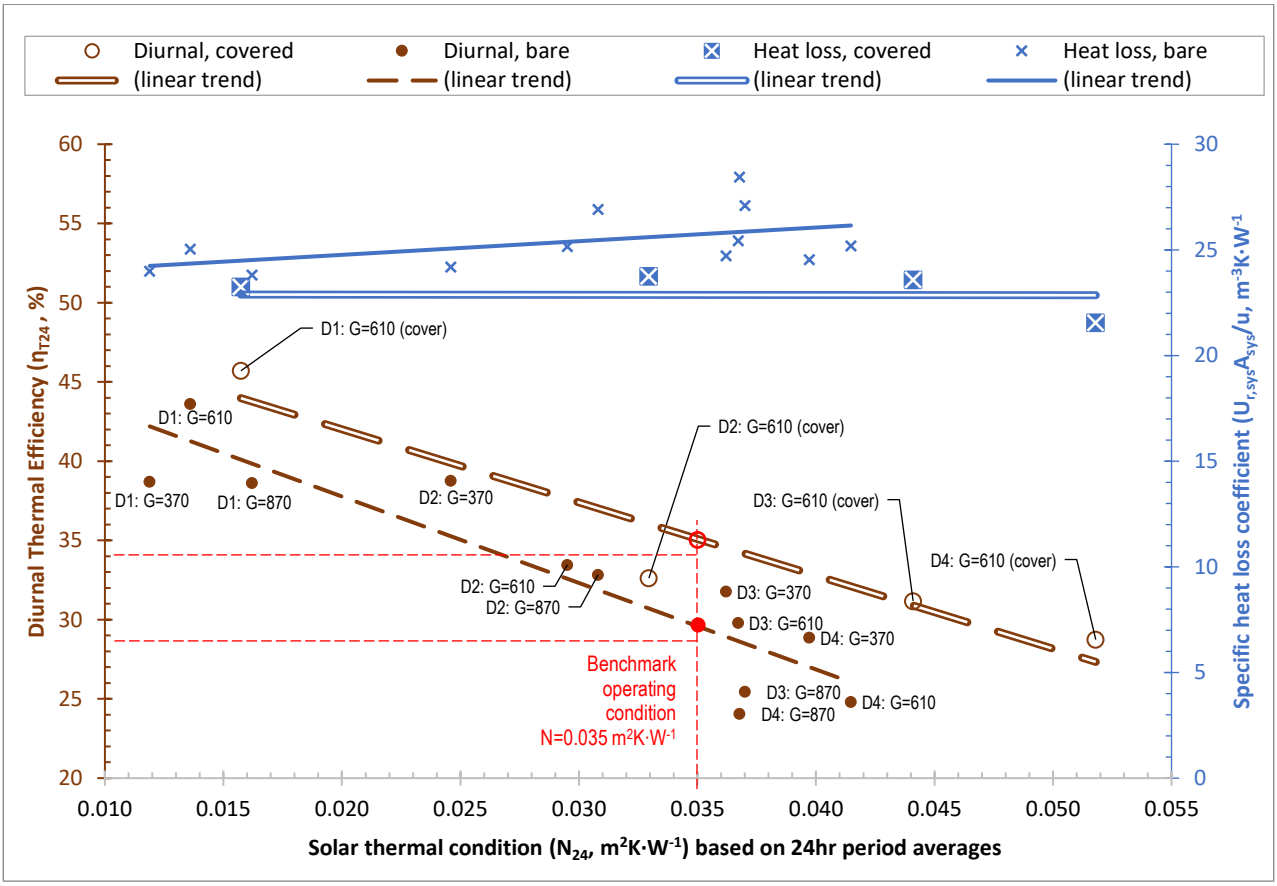

Figure 11: Measured diurnal thermal efficiencies and specific heat loss coefficients on Days D1, D2, D3 & D4 of testing

Measured diurnal thermal ($\eta_{T,24}$) efficiencies and volume specific heat loss coefficients ($U_{r,sys}A_{sys}/u$) are summarised on Figure 11. Whole-period results for each day (D1, D2, D3 & D4) of each test (irradiances G = 370, 610 & 870 W/m^2 with and without cover) are presented with reference to daily solar thermal condition (N_{24} calculated according to Equation 5 based on 24h average $\tilde{T}_3$ and $\tilde{T}_a$). Results show that single covered and bare absorber variants of the BIPV-PLVTD-ICSSWH prototype achieved diurnal efficiencies of $\eta_{T,24}$ = 35% and 29% respectively at the benchmark solar thermal condition (N=0.035 $m^2K \cdot W^{-1}$) which is in good agreement with model predictions.

Measured heat loss coefficients were $U_{r,sys}A_{sys}/u$ = 25.4 and 23.0 $W \cdot m^{-3}K^{-1}$ respectively for the bare absorber and single covered variants of the BIPV-PLVTD-ICSSWH, corresponding to 18h heat retention efficiencies of η_{ret} = 71% and 69% respectively. These values are broadly similar to those predicted by the theoretical model ($U_{r,sys}A_{sys}/u$ ≈ 20 $W \cdot m^{-3}K^{-1}$, refer to our study introduction paper, Part 1 of 2) and as expected, do not exhibit significant dependence upon temperature within the ranges examined. As predicted by the modelling results the heat loss coefficients demonstrate that the transparent cover provides only a small benefit (~10% $U_{r,sys}$ improvement or ~2%

extra η_{ret}) in respect of controlling overnight heat loss when used in tandem with a PLVTD. The model suggests that the cover would have a much larger effect if no PLVTD were employed which is why most ICSSWH collectors (which do incorporate thermal diodes) employ one or more transparent covers to control overnight heat loss.

3.4 Photovoltaic performance results

Measured open circuit voltages, short circuit currents, and fill factors for each string are shown on Figure 12. The same data for the whole module (formed by connecting the strings as a 5x series by 3x parallel module, see Figure 3 and discussion in Section 3.1) is shown on Figure 13.

Open circuit voltage under moderate to high irradiance conditions varied from V_{oc}=4.75±0.07 V per string at 25°C to a little less than 4V at 70°C (Figure 12a) and the maximum measured overall module open circuit voltage was V_{oc} = 5 x 4.75 = 24V (Figure 13). Corresponding voltage-temperature coefficients ($K_{V:T}$ = -0.36%/K for strings and $K_{V:T}$ = -0.38%/K for whole module) are very close to the manufacturers published data (single cell $K_{V:T}$ = -0.37%/K according to Bosch, 2010). A slight drop in open circuit voltage is apparent under low irradiance (G=370 W/m^2), corresponding to voltage-irradiance coefficient of $K_{V:G}$≈96%, broadly as expected.

Short circuit currents varied from I_{sc} = 0.4A for the worst string under low irradiance up to I_{sc} = 1.7A for the best string, and I_{sc} = 4.5 A for the whole module, under high irradiance (G=870 W/m^2). Calculated current-intensity relationships for individual strings were found to be in the range 23 < I_{sc}/(G·A) < 40 mA/W which is lower than the expected 45 mA/W implied by manufacturer's performance data (Bosch, 2010). This is largely attributed to partial delamination of the bonded transparent covers (which gave cells a slightly whitened or faded appearance, implying optical losses) and also due to accidental cell damage (cracks etc which reduce active collection area and introduce electrical resistances). Comparison of short circuit currents measured on 20 & 25 May against those measured on 16 May (see Figure 12b) clearly indicates a performance drop for Strings 2 & 3 which is consistent with cells having suffered permanent damage such as thermo-mechanical stresses causing cells to crack. Smaller performance drops are also evident for Strings 1, 8, 9 and 10 and are consistent with optical losses caused by cover delamination. Whole-module test data (Figure 13) indicates that the current-temperature effect is $K_{I:T}$ ≈ -0.04%/K (based on trendline gradients) or $K_{I:T}$≈-0.07%/K (across the temperature range) with an abrupt non-linear

step in behaviour at a critical temperature ($T_1 \approx 50°C$ for most tests but $T_1 \approx 70°C$ for the high irradiance test). Current-temperature effects are usually linear and of relatively small positive magnitudes ($K_{I:T} \approx {}^{+}0.03\%/K$ expected for a single cell according to Bosch, 2010) but in this case the effect is significantly negative and non-linear, consistent with PV cell fractures induced by thermal stress. The absorber laminate is formed of a mixture of metal (thermal diode evaporator), ceramic (PV cells), and polymeric (bonded transparent cover) elements which all have different thermal expansion coefficients. This induces thermal stress which causes cracks to form when the absorber temperature increases due to the metal and polymeric elements expanding more quickly than the fragile PV cells. The cracks open when the absorber is hot, which causes fractured parts of the PV cells to be electrically isolated from the strings. The cracks close again when the absorber cools, allowing fractured parts to reconnect to the string (albeit imperfectly).

A typical 8-cell string achieved fill factors of FF=74% during high irradiance tests and FF=77% during low irradiance tests (Figure 12) which is consistent with the typical 75%<FF<85% range reported in the literature (refer to Section 2.2 of our study introduction paper, Part 1 of 2). Whole-module tests (Figure 13) exhibited a wider range of measured fill factors (66%<FF<81%) but average values were very similar to those measured for individual strings. As expected, the lowest measured fill factors typically correspond to the highest irradiances when series resistances (eg soldered connections, tabbing, and cables) have the greatest influence. As expected, measured fill factors do not appear to exhibit any significant temperature dependence.

Measured current-voltage and load-power curves for the whole module are presented on Figures 14 & 15 respectively. As expected, voltage reduces with increasing temperature and current reduces with reducing irradiance. The optimal load conditions indicated by the peaks on Figure 15 were used during the experiments as a guide to enable periodic adjustment of the load resistance (R_E) to ensure continuous operation close to the maximum power point. The highest measured maximum power point power output ($q_{E,mpp}$=75W, FF=70%, R_E=5Ω) occurred whilst the tank was close to its lowest temperature under the high irradiance condition (G=870 W/m^2 without cover, T_3=17°C). The lowest measured output ($q_{E,mpp}$=24 W, FF=72%, R_E=14Ω) occurred whilst the tank was close to its maximum temperature under the low irradiance condition (G=370 W/m^2 without cover, T_3=40°C). Figure 14 indicates that a reduction

464 in I_{sc} occurs when the transparent cover is added (13% reduction for $T_3 \approx 17°C$ cold
465 tank case, 6% reduction for $T_3 \approx 50°C$ hot tank case) but the exact magnitude of the
466 optical loss (expected to be ~8%) is impossible to determine owing to superimposed
467 current-temperature effects. Figure 16 shows how the maximum power point electrical
468 efficiency of the whole PV module varies with absorber temperature from maxima at
469 $T_1 \approx 25°C$ of $\eta_{E,mpp}$ 11.4% (without cover) and $\eta_{E,mpp}$ 9.8% (with cover) to minima of
470 $\eta_{E,mpp}$ 5.6% (without cover at $T_1 \approx 89°C$) and $\eta_{E,mpp}$ 5.9% (with cover at $T_1 \approx 62°C$).
471 Measured low temperature efficiencies for the covered collector are lower than
472 expected ($\eta_{E,mpp}$ 10.9% predicted by the theoretical model, refer to Figures 7 and 9 of
473 our study introduction paper, Part 1 of 2). This reduction can be explained by the
474 accidental cell damage which occurred during fabrication and by the optical losses
475 caused by partial delamination of the bonded transparent cover during initial tests.
476 Measured efficiencies at higher temperatures deviate further from model predictions
477 owing to the higher than expected current-temperature effect which appears to be
478 associated with thermal stress cracks in the PV cells (see discussion above).
479

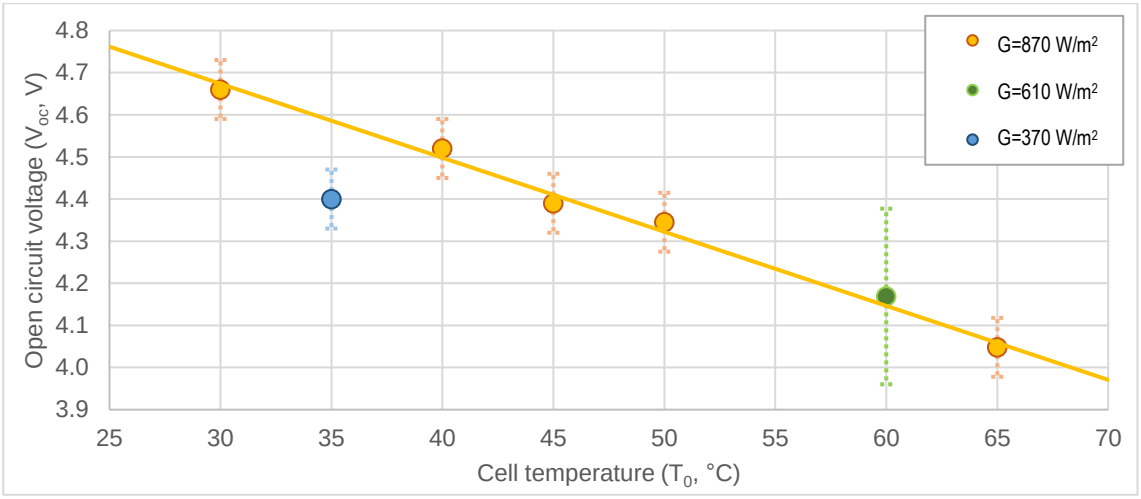

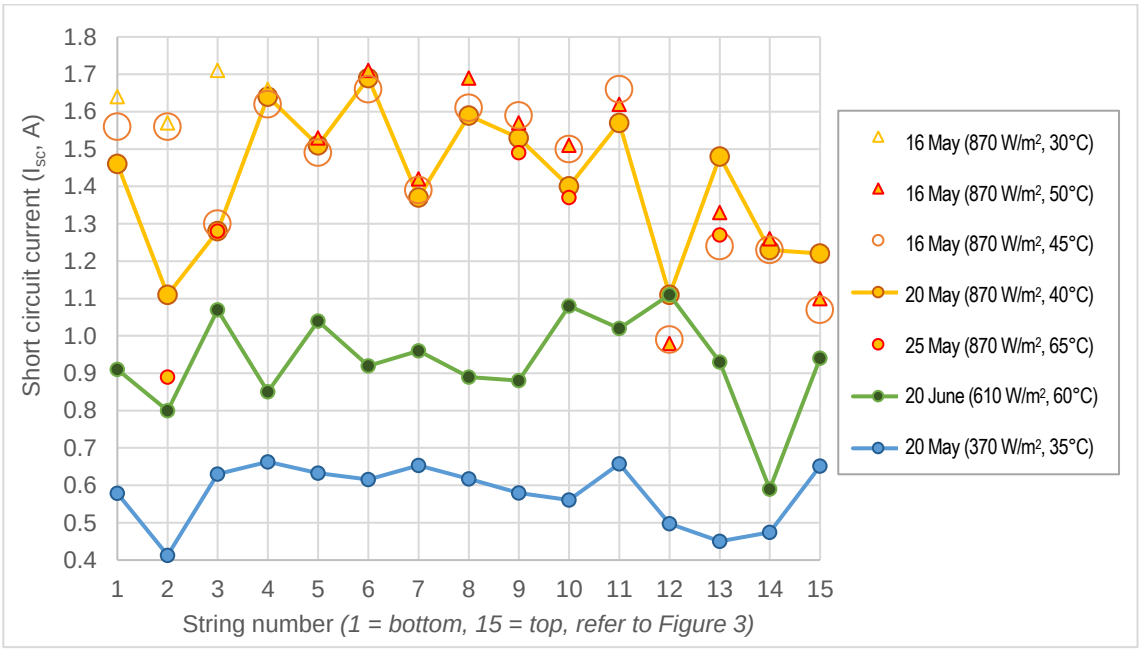

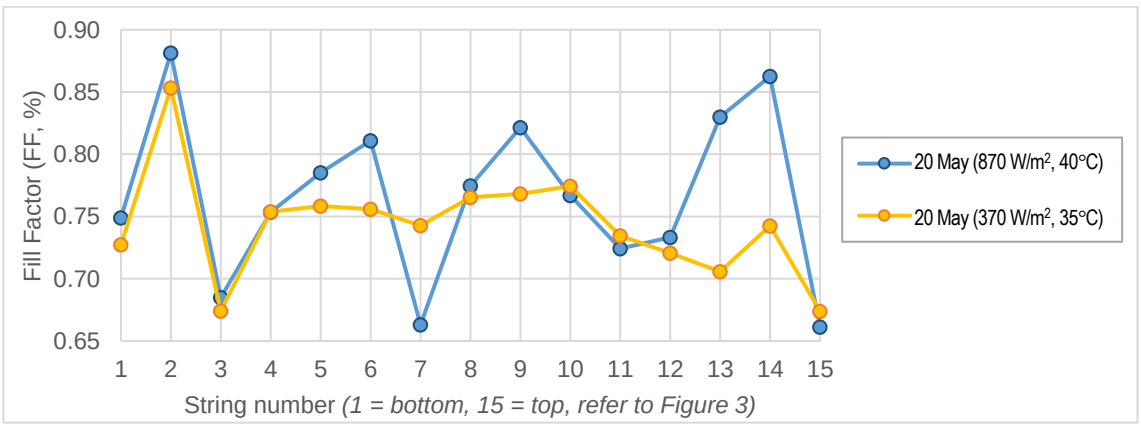

a) Upper graph shows temperature dependence of average measured open circuit voltage. Vertical error bars represent the observed range of voltage variation between different strings.

b) Middle graph compares measured short circuit currents for each string. Measurements were made at various different temperature and irradiance conditions and on various dates.

c) Lower graph compares measured Fill Factors for each string under high and low irradiance conditions.

Figure 12: Results of photovoltaic measurements on individual 8-cell strings

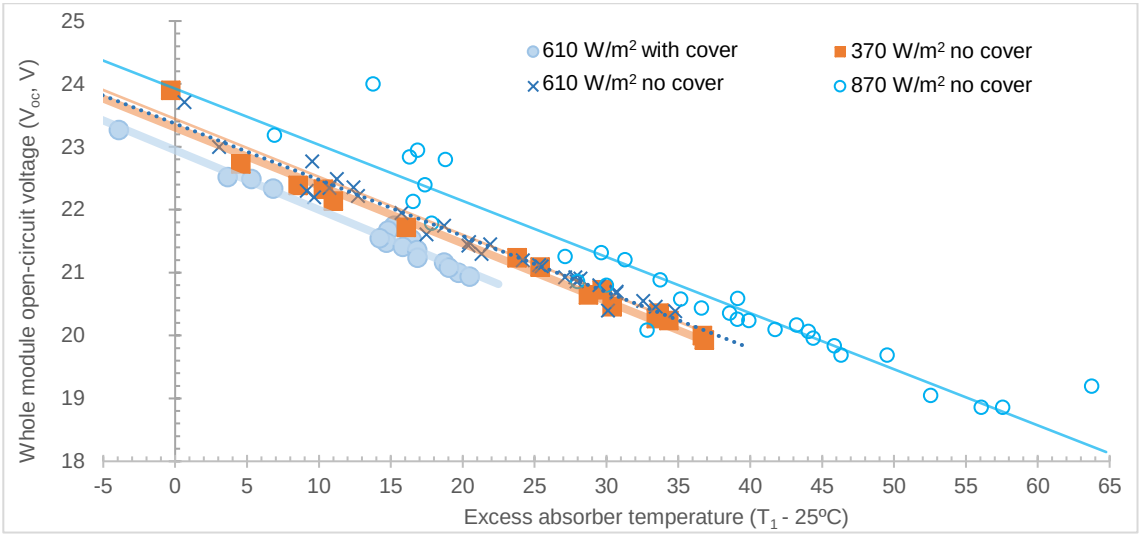

490

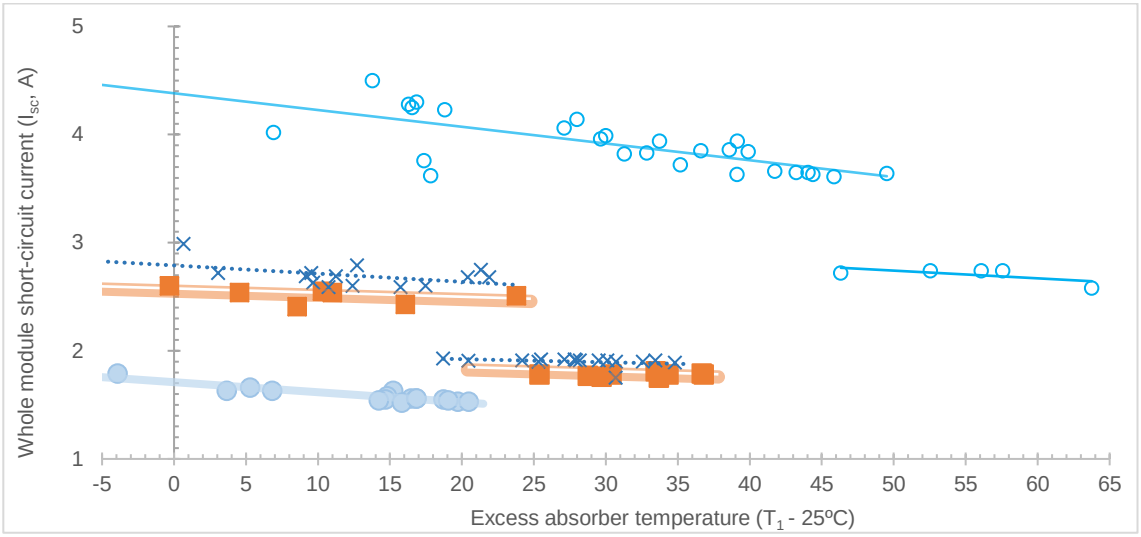

491

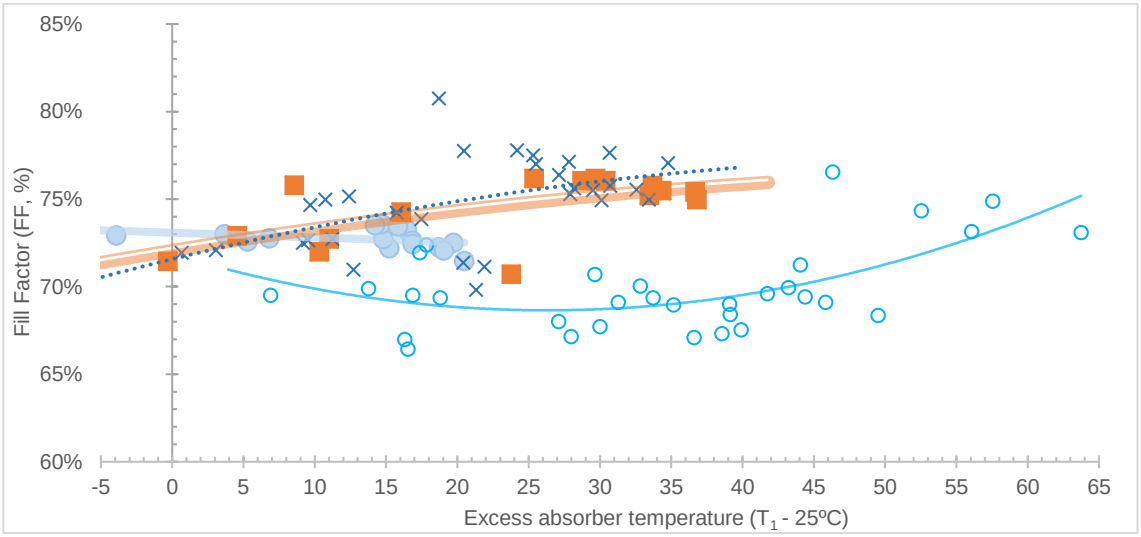

492
493
494 a) Upper graph shows temperature dependence of measured open circuit voltage.
495 b) Middle graph shows temperature dependence of measured short circuit current.
496 c) Lower graph compares shows temperature dependence of measured Fill Factors.

497 The x-axis corresponds to the absorber temperature less the Standard Test Condition (STC) reference temperature of 25°C.

498 ***Figure 13: Results of photovoltaic measurements on the whole module***

499

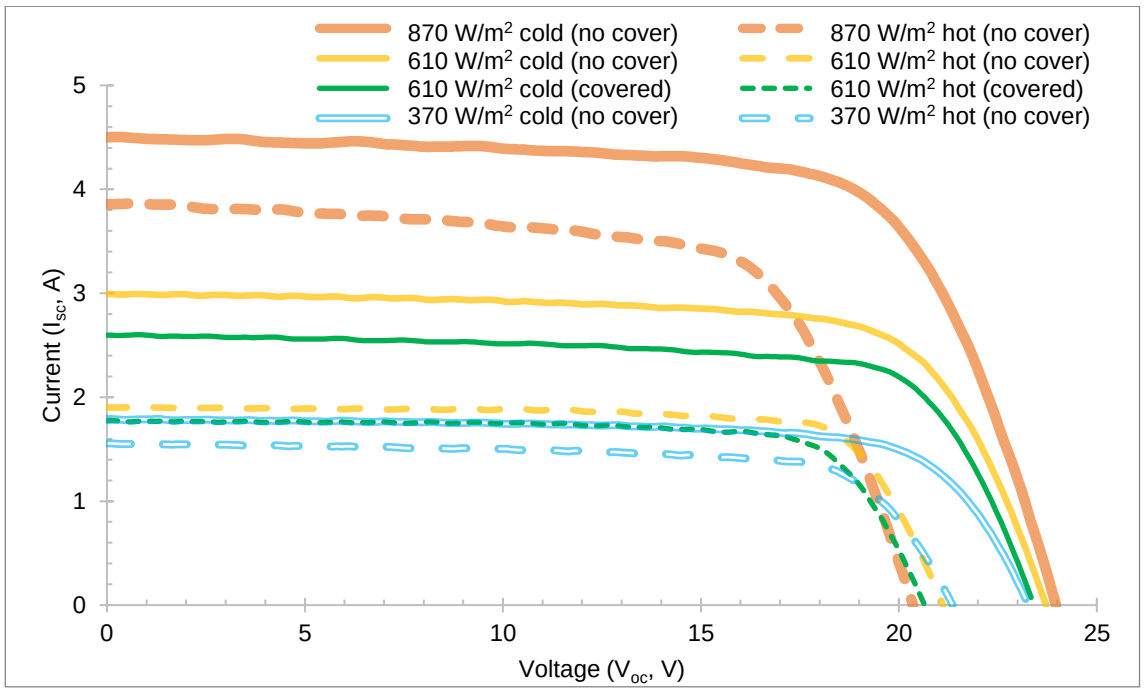

500
501 ***Figure 14: Current-voltage characteristics of the photovoltaic module under a variety of different conditions***
502

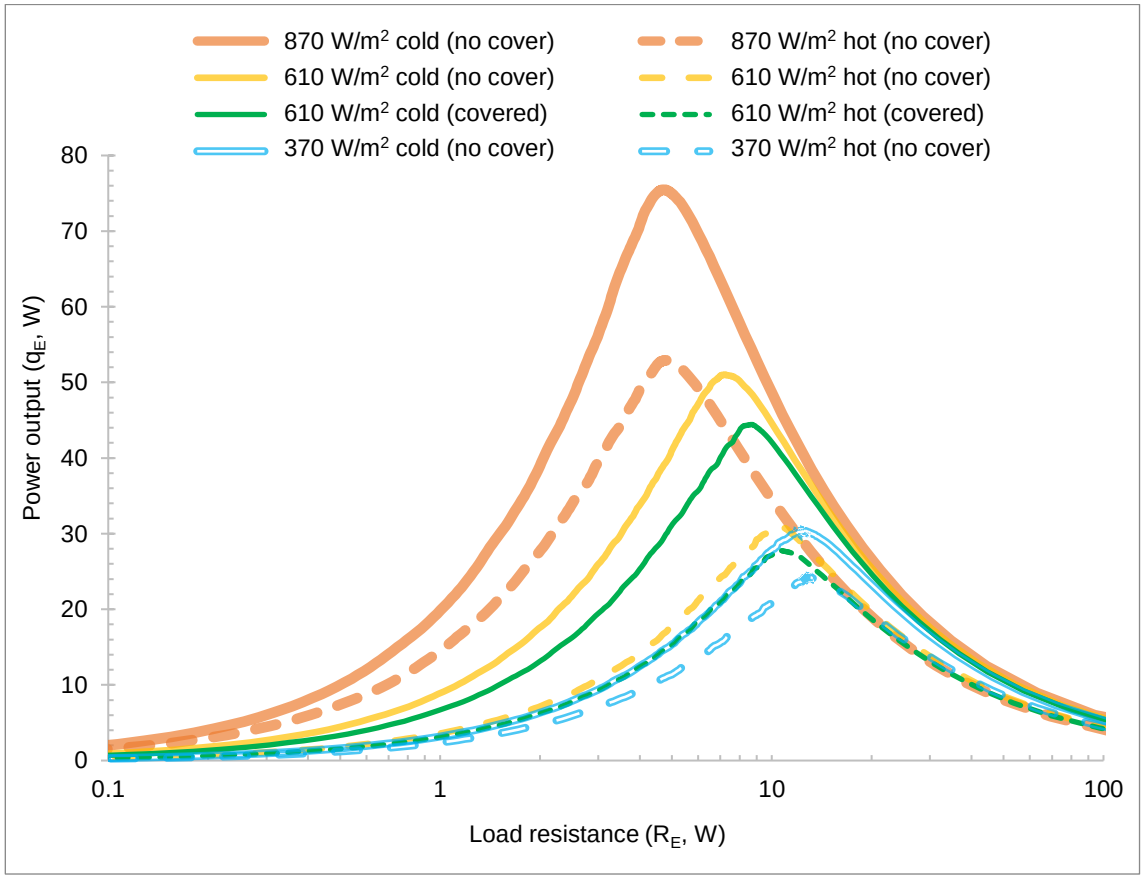

503
504 ***Figure 15: Load-Power characteristics of the photovoltaic module under a variety of different conditions***

505

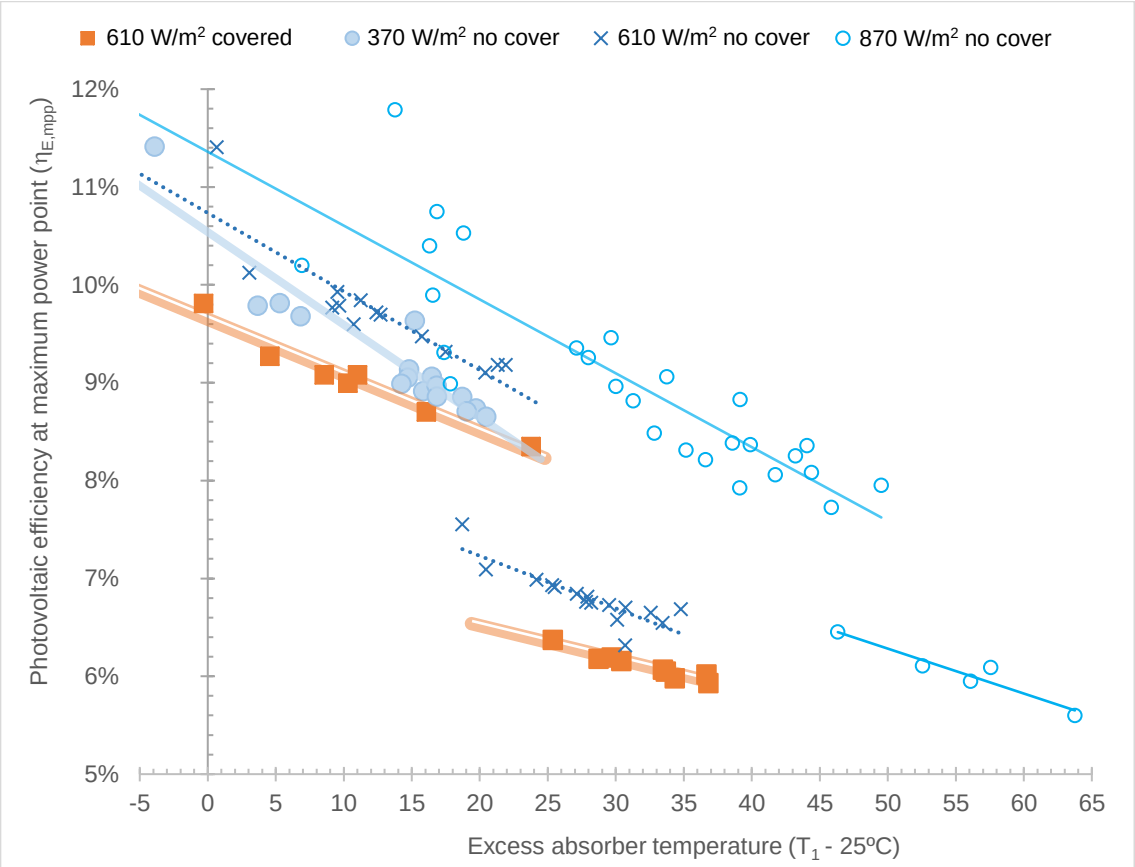

Figure 16: Variation in measured maximum power point photovoltaic efficiency with temperature and irradiance

3.5 Conclusions concerning model validity

The measured thermal behaviour of the BIPV-PLVTD-ICSSWH prototype is in good agreement with the theoretical model. Measured maximum and minimum water storage tank temperatures are typically within ±3°C of modelled values, solar thermal collection efficiencies are typically within ±3% of modelled values, and specific overnight heat loss coefficients are typically within ±3 $W \cdot m^{-3} K^{-1}$ of modelled values. The photovoltaic performance of the prototype was somewhat worse than expected owing to accidental damage to PV cells during fabrication and also due to delamination of the bonded transparent cover. The current-temperature relationship was the opposite of that expected and exhibited non-linearities which appear to be the result of PV cell cracks induced by thermal stress. Despite these issues, measured voltage-temperature trends, the current-irradiance relationship, and fill factors, were all broadly as expected, indicating that the core theoretical model is valid.

4 Building integration and future concept development

Development of the BIPV-PLVTD-ICSSWH approach from concept to reality requires an appreciation of the available energy resource, the key operating principles, and a validated theoretical understanding of device behaviour, as established through the parametric modelling and experimental work presented in this two-part study. Future design work and realisation of pre-commercial prototypes requires consideration of the application context (such as the thermal and electrical energy demands served by the system) as well as the practical constraints and opportunities associated with integration into conventional architectural and building services systems.

4.1 Building energy demands

Total energy use in buildings is determined by a combination of thermal demands and occupier electrical loads. Thermal demands for space heating and cooling depend upon local climatic conditions, building envelope thermal insulation, solar shading, and occupancy rates, but tend to be proportional to total envelope area (façades plus roof, through which heat losses and gains occur). Occupier electrical loads and domestic hot water demands depend upon user needs and occupancy rates but tend to be proportional to floor area (Bellusi et al., 2019). For any PV/T system to be useful, there must be a demand for both electricity and low-grade heat, and the solar collectors must be coupled to the building's heating and electrical systems (Affolter et al., 2006; Zondag, 2008; Calise et al., 2016).

Demands for electricity are often reasonably well matched to the diurnal and seasonal availability of solar resources, especially in hot and sunny climates where summertime cooling demands are significant (Sorgato et al., 2018). Even when supply and demand are ill-matched, excess electricity can often be utilised effectively by exporting it to the mains electricity grid or storing it in batteries (Kats and Seal, 2012). Domestic hot water demand is typically reasonably constant throughout the year and can be an effective way of utilising the heat produced by PV/T systems provided that the heat can be delivered at a sufficiently high temperature (with consequent sacrifice of PV efficiency, as demonstrated by Figure 16) and stored in sufficient quantity without significant heat losses. Whilst the required temperatures can be readily achieved in warm and sunny climates, it is more difficult in cold and windy climates, and the provision of heat loss control features (such as single or double transparent covers) reduces PV efficiency and also increases the risk of stagnation overheating when hot water demands are low. Space heating is typically the largest thermal demand for buildings in cool climates and can be accomplished using relatively low heat delivery

temperatures in many cases (eg underfloor heating) but unfortunately, the greatest need (during winter) does not occur when the best solar resource is available (during summer). This issue is clearly problematic for latitude tilted and near-horizontal (eg roof mounted) collectors which typically receive 2 to 5 times more insolation in summer than they do in winter (refer to Table 1 in our study introduction paper, Part 1 of 2). The seasonal solar resource variance is however much less pronounced in the case of facade integrated collectors. Seasonal mismatches between solar resource availability and heat demands can, in principle, be dealt with by using thermal storage but the vessels required tend to be prohibitively large and supply temperatures limited (too low for domestic hot water or conventional hydronic heating systems employing radiators). These issues are often cited as major barriers against the widespread adoption of PV/T and other types of solar space heating.

4.2 Heat pump integration

More than a decade ago, Zondag (2008) suggested that: "*More experience should be obtained for unglazed PV/T collectors combined with a heat pump, since this may be a promising development for the future*". Subsequent research investigating the use of low temperature heat from PV/T systems as a thermal source for heat pumps appears to have been somewhat scarce (Good et al., 2015; Qu et al., 2016; Calise et al., 2016) until very recently (Lazzarin et al., 2019; Shao et al., 2020; Yao et al., 2020; Zhou et al., 2020). Stagnation overheating during times of low thermal demand and transient overheating disrupting compressor start-up are common themes in these recent studies. Overheating in PV/T heat pump systems not only reduces PV electrical efficiency and increases risk of damage to collectors (especially those featuring transparent covers and air gaps to reduce heat losses) but also poses problems for heat pump operation (eg excessive refrigerant pressures which impair compressor function and damage seals etc). As demonstrated in our study introduction paper (Part 1 of 2) the BIPV-PLVTD-ICSSWH concept provides a passive means of preventing overheating and stabilising temperature fluctuations, thus representing a promising avenue for further development.

4.3 Façade integration

The BIPV-PLVTD-ICSSWH concept is intended to be integrated into building facades and is particularly relevant for multi-storey buildings where the roof area is small compared to the total façade area and the usable floor area. Whilst vertical façade-mounted solar collectors generally receive lower levels of irradiance than tilted roof-mounted collectors, and are more likely to be subjected to shading from surrounding

buildings and trees, the total solar resource incident on multi-storey building facades is commonly greater than that incident on the roof owing to the much larger overall area. In new buildings and major refurbishments, façade mounted solar collectors should ideally be an integral part of the façade design and construction process (rather than a bolt-on addition) for reasons of aesthetics, economics and maintainability. Façade integration of a BIPV-PLVTD-ICSSWH involves a variety of design drivers and constraints, some of which are common to conventional BIPV installations, and others which primarily relate to the ICSSWH element. These include:

- **Visual appearance** is recognized as a crucial consideration for (and potential barrier against) widespread adoption of BIPV and BISTS. Absorber surface colours and planar forms can be manipulated to achieve architectural expression or alternatively to "camouflage" collectors if preferred (Tripanagnostopoulos et al., 2000; Affolter et al., 2006; and COST, 2015). The absorber surface and any transparent covers need to be aesthetically appropriate and their dimensions need to be compatible with the building facade's structural grid.
- **Relatively high capital costs** of BISTS are often seen as prohibitive. However, collector components (such as insulation, exterior weather facing surface, structure) can replace elements of the façade resulting in net cost reductions compared to bolt-on solutions. Collectors also produce energy which means that the façade will partially or wholly "pay for itself" over time.
- **Façade zone and structural compatibility** constraints may limit overall BIPV-PLVTD-ICSSWH depth or limit tank volumes. The form of the device inherently needs to be slender in order to fit within the depth of conventional façade constructions. The weight of the stored water in the tank will impose significant structural loads on façade structural elements and/or floor slab edges in addition to self-weight and wind loads, hence a compromise between desired storage capacity and structural loading constraints must be sought. Fixings and pipe penetrations must not compromise the integrity of the structure and should ideally be readily accessible for inspections and maintenance.
- **Electrical compatibility** with conventional cabling and inverter arrangements is important to ensure interoperability with existing market solutions. PV panel voltages and shading tolerance needs to be considered. Micro-inverters may be a good solution in these respects. Cable routes should be accessible and avoid clashes with structural elements.

- **Thermal compatibility** with conventional façade thermal insulation, condensation control, and ventilation strategies. Integrated BIPV-PLVTD-ICSSWH collectors must not significantly add to building heat loads when the stored water is hot (eg during summer). Likewise, the collectors and associated pipework must not compromise the envelope by causing thermal bridging or creating condensation problems.
- **Protection of PV cells** against mechanical and thermal stress, weathering and humidity, as well as electrical isolation from the collector main body (metal). The issue of thermal stress should not be underestimated, especially given the problems encountered with temperature induced PV cell cracking observed during the experiments undertaken in the present study.
- **Robustness and stability** of construction materials and joints/interfaces with due regard to operating and stagnation temperatures; thermal expansion stresses; exposure to precipitation (rain, snow, hail, and atmospheric moisture); wind loads, and UV radiation. The water storage tank must withstand the self-weight of the water it contains (together with any applied water pressure) and the PLVTD must maintain a reliable vacuum, thus these components require dimensional stability to ensure negligible leak risk.
- **Maintenance** of collector components needs careful consideration. Components requiring regular maintenance should be accessible from inside the building. Where this proves impossible, the cost and complexity of access to façade mounted collectors on tall building can be minimized by utilizing available façade access equipment (window cleaning cradles etc) and ensuring that façade access strategies consider collector maintenance.
- **Other façade design requirements** such as fire protection, fire safety of component materials, and sound insulation may also be relevant factors in the design of a viable BIPV-PLVTD-ICSSWH system.

The abovementioned opportunities and constraints were considered insofar as possible during the design of the prototype examined in this study, but further work will be required to refine the concept through consultation with architects, façade engineers and other construction professionals. Issues concerning costs, structural loading and material robustness are the main areas of design risk to be addressed in future studies.

One of the most unique aspects of the BIPV-PLVTD-ICSSWH concept is the thermal diode component. Whilst our experimental prototype functioned adequately during the

laboratory tests, the pumped evaporator wetter mechanism was found to be problematic in respect of vacuum leakage, excessive power consumption, and uneven wetting of the evaporator plate which impaired the forward mode thermal diode performance (described in more detail by Pugsley et al., 2017 & 2020). It was also found that the strut array support structure inside the PLVTD (see Figure 4) was difficult to fabricate. Further development of the PLVTD component will focus on the use of passive evaporator wetting mechanisms (such as capillary wicking) and trialling alternative structural support arrangements.

5 Conclusions

This two-part study examined an alternative space-and-energy-efficient approach to BIPV/T which combines BIPV, ICSSWH, and PLVTD concepts. Our first paper (Part 1 of 2) established the novelty and rationale for the concept and used theoretical modelling to predict behaviour. The present paper (Part 2 of 2) described the realisation of a prototype; presented results of multi-day solar simulator laboratory tests to validate the theoretical model; identified key practical considerations and areas for future design improvement; and discussed the key benefits and challenges associated with integrating BIPV-PLVTD-ICSSWH concepts into NZEB facades as part of global decarbonisation efforts to tackle the climate crisis.

The vertically oriented BIPV-PLVTD-ICSSWH prototype (A_1=1m^2 absorber & PLVTD area with 75% PV cell coverage; x=70mm PLVTD depths; u=0.1m^3 hot water store) was tested using a solar simulator under representative scenarios (6h exposure at G=370, 610 and 870 W/m^2 with and without transparent cover followed by 18h darkness, repeated for 4 daily cycles) to examine multi-day behaviour. Measurements quantified time variant absorber ($19<T_1<89$°C) and stored water ($17<T_3<61$°C) temperatures; instantaneous solar thermal ($26<\eta_T<68$%) and photovoltaic ($5.6<\eta_E<11.8$%) collection efficiencies; whole-module temperature dependent current-voltage characteristics ($19<V_{oc}<24$V, $K_{V:T}$ = -0.38%/K, $1.5<I_{sc}<4.5$A, $K_{I:T}$ ≈ -0.04%/K, $66<FF<81$%); heat loss coefficients ($21<U_{r,sys}A_{sys}/u<29$W·m^{-3}K^{-1}); and diurnal thermal efficiencies ($24<\eta_{T,24}<46$%). Key findings were as follows:

- From a common starting condition of $T_3 \approx T_a \approx 17$°C, water storage tank temperatures were observed to reach Day 4 maxima of T_3 = 61, 53, 40 and 57°C respectively for G=870, 610 and 370 W/m^2 irradiance tests without transparent cover and G=610 W/m^2 irradiance tests with transparent cover.
- Solar thermal efficiencies with and without the transparent cover were found to be $\eta_{T,col}$=60% and 58% respectively under zero heat loss conditions

($N=0.0\ m^2K\cdot W^{-1}$), falling to $\eta_{T,col}$=49% and 40% respectively at the benchmark solar thermal condition ($N=0.035\ m^2K\cdot W^{-1}$).

- Measured overnight heat loss coefficients were $U_{r,sys}A_{sys}/u$ = 23.0 and 25.4 $W\cdot m^{-3}K^{-1}$ respectively with and without the transparent cover, corresponding to 18h heat retention efficiencies of $\eta_{T,ret}$ 71% and 69%.
- Compared to modelled values, measured water storage tank temperatures were typically within ±3°C, solar thermal collection efficiencies were typically within ±3%, and specific overnight heat loss coefficients were typically within ±3 $W\cdot m^{-3}K^{-1}$, indicating that the theoretical model is suitably valid to enable thermal performance predictions across diurnal and seasonal timescales.
- Overall maximum power point PV module efficiencies were observed to reduce with increasing absorber temperature from $\eta_{E,mpp}$ = 11.4% (at T_1≈25°C) to 5.6% (at T_1≈89°C) without transparent cover. Adding the transparent cover reduced performance to $\eta_{E,mpp}$ = 9.8% (at T_1≈25°C). Allowing for issues associated with PV cell cracks and transparent cover delamination, the measured trends in PV performance were broadly as expected, indicating that the core elements of the theoretical model are valid.

Whilst the experimental prototype functioned adequately during the laboratory tests, opportunities for design refinements have been identified to support realisation of pre-commercial prototypes focussed on integration into conventional architectural facades and building services systems, including:

- Use of passive evaporator wetting mechanisms and alternative internal structural support arrangements within the PLVTD.
- Optimisation of integrated thermal storage sizing to accommodate diurnal and seasonal supply and demand mismatches; provide stable temperatures to support operation as a thermal source for heat pumps; minimise potential for stagnation overheating during hot and sunny low heat demand periods; and satisfy structural loading constraints associated with weight of storage media.

The BIPV-PLVTD-ICSSWH façade concept provides a passive means of addressing overheating and thus represents a promising avenue for further development. Issues concerning costs, structural loading and material robustness do however need to be addressed as part of a multi-disciplinary design approach to support realisation of NZEBs as part of global efforts to tackle the climate crisis.

Acknowledgements

This research was enabled in its early stages by studentship funding support from the Northern Ireland Department for the Economy. The work was subsequently progressed with funding support from SolaForm Ltd and was completed as part of the "SolaNetwork" project funded by the UKRI Engineering and Physical Sciences Research Council (EP/T004819/1). The authors would also like to thank networking support funded by the European Union FP7 COST Action TU1205 "Building Integration of Solar Thermal Systems".

Nomenclature

Latin symbols

A	Surface area [m^2]
c_p	Specific heat capacity at constant pressure [$J \cdot kg^{-1} K^{-1}$]
FF	Photovoltaic Fill Factor [%]
G	Solar irradiance [$W \cdot m^{-2}$]
H	Solar insolation [$MJ \cdot m^{-2}$]
I	Electrical current [A]
K	Photovoltaic performance correction coefficients [% or %/K]
M	Mass [kg]
N	Solar Thermal Condition [$m^2 \cdot K \cdot W^{-1}$]
q	Thermal or electrical power [W]
R	Thermal or electrical resistance [$K \cdot W^{-1}$]
t	Time [s]
T	Temperature [°C]
$\tilde{T}_{[t]}$	Average temperature, during time period [°C]
u	Volume [m^3]
U	Thermal conductance or heat transfer coefficient [$W \cdot m^{-2} K^{-1}$]
V	Electrical voltage [V]
x	Distance along an axis which is parallel to the PLVTD depth [m]
y	Distance along horizontal axis perpendicular to PLVTD depth [m]
z	Distance along an axis which is perpendicular to x and y axes [m]

Greek and other symbols

α	Absorptivity
ΔT	Temperature difference [°C]
η	Efficiency [%]
τ	Transmissivity

Subscripts

0	Photovoltaic cells
1	Planar Liquid-Vapour Thermal Diode, Plate 1 which is the evaporator in forward mode

2	Planar Liquid-Vapour Thermal Diode, Plate 2 which is the condenser on forward mode
3	Hot water storage tank
4	Sidewalls of the Planar Liquid-Vapour Thermal Diode
5	External surface of the solar absorber
6	Transparent element covering solar absorber
0a	Between PV cells and ambient environment
03	Between PV cells and hot water storage tank
1a	Between solar absorber and ambient environment
12	Between (or average of) the two plates
15	Between the PLVTD and the external surface of the solar absorber (through the laminate)
24	Diurnal period of 24 hours
3a	Between water storage tank and ambient environment
3ia	Between water storage tank and ambient environment through insulation
4ia	Between insulated PLVTD sidewalls and ambient environment
56	Across the air gap between the solar absorber and transparent cover
a	Ambient environment
col	Collection (period of solar absorber illumination, eg daytime)
E	Electrical
f	Forward mode
load	Connected electrical load
mpp	Maximum Power Point
oc	Open circuit
P	Pump
PV	Photovoltaic
r	Reverse mode
ret	Retention (period without solar absorber illumination, eg night-time)
sc	Short circuit
STC	At Standard Test Conditions
sys	Whole system
T	Thermal
I:T	Current-Temperature relationship
V:T	Voltage-Temperature relationship
V:G	Voltage-Irradiance relationship

Abbreviations

AM	Air Mass index
BIPV	Building Integrated PhotoVoltaics
BISTS	Building Integrated Solar Thermal Systems
ICSSWH	Integrated Collector-Storage Solar Water Heater
mc-si	Mono-crystalline silicon
NZEB	Net Zero Energy Building
nZEB	Nearly Zero Energy Building
PLVTD	Planar Liquid-Vapour Thermal Diode
PV/T	Photovoltaic-Thermal
STC	Standard Test Conditions (for PV cells and modules)

References

Affolter, P., Eisenmann, W., Fechner, H., Rommel, M., Schaap, A., Soerensen, H., Tripanagnostopoulos, Y. Zondag, H. (2006). PVT Roadmap – European guide for the development and market introduction of PV-Thermal technology. Petten, Netherlands: Energy research Centre of the Netherlands (ECN). Available at: <http://www.pvtforum.org/pvtroadmap.pdf> [Last Accessed 10 January 2014]

Arya, F., Moss, R., Hyde, T., Shire, S., Henshall, P., Eames, P. (2018). Vacuum enclosures for solar thermal panels Part 2: Transient testing with an uncooled absorber plate. Solar Energy 174, 1224-1236

Belussi, L., Barozzi, B., Bellazzi, A., Danza, L., Devitofrancesco, A., Fanciulli, C., Ghellere, M., Guazzi, G., Meroni, I., Salamone, F., Scamoni, F., Scrosati, C. (2019). A review of performance of zero energy buildings and energy efficiency solutions. Journal of Building Engineering 25 (2019) 100772

Bosch (2010). High performance – Stable yields. Bosch Solar Cell M 2BB. [Last accessed: 10 September 2016]. Arnstadt, Germany: Bosch Solar Energy AG. Available at: <http://www.bosch-solarenergy.com>.

Calise, F., d'Accadia, M, Figaj, R., Vanoli, L., (2016). A novel solar-assisted heat pump driven by photovoltaic/thermal collectors: Dynamic simulation and thermoeconomic optimization. Energy 95, 346-66

COST Action TU1205 (2015). Overview of BISTS state of the art, models and applications. ISBN: 978-9963-697-16-8. Cyprus University of Technology / European Union Horizon 2020.

Drosou, V., Tsekouras, P., Oikonomou, T., Kosmopoulos, P., Karytsas, C. (2014). The HIGH-COMBI project: High solar fraction heating and cooling systems with combination of innovative components and methods. Renewable and Sustainable Energy Reviews 29 (2014) 463–472

Dupeyrat, P., Menezo, C., Rommel, M., Henning, H. (2011). Efficient single glazed flat plate photovoltaic-thermal hybrid collector for domestic hot water systems. Solar Energy 85, 1457-68

Fayaz, H., Rahim, N., Hasanuzzaman, M., Nasrin, R., Rivai, A. (2019) Numerical and experimental investigation of the effect of operating conditions on performance of PVT and PVT-PCM. Renewable Energy 143 (2019) 827-841

Good, C., Andresen, I., Hestnes, A. (2015). Solar energy for net zero energy buildings – A comparison between solar thermal, PV and photovoltaic–thermal (PV/T) systems. Solar Energy 122, 986–96

Hasanuzzaman, M., Malek, A., Islam, M., Pandey, A., Rahim, N. (2016). Global advancement of cooling technologies for PV systems: A review. Solar Energy 137 (2016) 25-45

Kats, G., Seal, A. (2012). Buildings as Batteries: The Rise of 'Virtual Storage'. The Electricity Journal 25 (10) 59-70 http://dx.doi.org/10.1016/j.tej.2012.11.004

Kazemian, A., Hosseinzadeh, M., Sardarabadi, M., Passandideh-Fard, M. (2018). Experimental study of using both ethylene glycol and phase change material as coolant in photovoltaic thermal systems (PVT) from energy, exergy and entropy generation viewpoints. Energy 162 (2018) 210-223

Krauter, S. (2004). Development of an integrated solar home system. Solar Energy Materials & Solar Cells 82 (2004) 119–130

Lazzarin, R., Noro, M. (2019). Photovoltaic/Thermal (PV/T) / ground dual source heat pump: optimum energy and economic sizing based on performance analysis. Energy and Building AIP (https://doi.org/10.1016/j.enbuild.2020.109800)

Muhumuza, R., Zacharopoulos, A., Mondol, J., Smyth, M., Pugsley, A., Giuzio, G., Kurmis, D. (2019). Experimental investigation of horizontally operating thermal diode solar water heaters with differing absorber materials under simulated conditions. Renewable Energy, Volume 138, August 2019, Pages 1051-1064

NASA - National Aeronautics and Space Administration (2019). Data Access Viewer for Prediction of Worldwide Energy Resource (POWER) Project funded through the NASA Earth Science/Applied Science Program. Hampton, USA: Langley Research Center (LaRC). Available at: < https://power.larc.nasa.gov/data-access-viewer/ > [Last accessed: 07/10/19].

Pugsley, A., Mondol, J., Smyth, M., Zacharopoulos, A., Di Mattia, L. (2016). Experimental characterisation of a flat panel integrated collector-storage solar water heater featuring a photovoltaic absorber and a planar liquid-vapour thermal diode. Proceedings of 11th ISES EuroSun Conference: Palma (Mallorca), Spain from 11 to 14 October 2016. Martinez, V. & Gonzalez, J. (eds.).

Pugsley, A. (2017). Theoretical and experimental analysis of a novel flat photovoltaic-thermal solar water heater with integrated energy storage via a planar liquid-vapour thermal diode. Ulster University PhD Thesis (uk.bl.ethos.713462) published July 2017.

Pugsley, A., Zacharopoulos, A., Mondol, J., Smyth, M. (2019). Theoretical and experimental analysis of a horizontal Planar Liquid-Vapour Thermal Diode (PLVTD). International Journal of Heat and Mass Transfer 144 (2019) 11866

Pugsley, A., Zacharopoulos, A., Mondol, J., Smyth, M. (2020). Vertical Planar Liquid-Vapour Thermal Diodes (PLVTD) and their application in building façade energy systems. Applied Thermal Engineering (submitted for publication 01/2020, under review)

Qu, M., Chen, J., Nie, L., Li, F., Yu, Q., Wang, T. (2016). Experimental study on the operating characteristics of a novel photovoltaic/thermal integrated dual-source heat pump water heating system. Applied Thermal Engineering 94, 819–26

Shao, N., Ma, L., Zhang, J. (2020). Experimental investigation on the performance of direct-expansion roof-PV/T heat pump system. Energy 195 (2020) 116959

Smyth, M., Eames, P. Norton, B. (2003). Heat Retaining Integrated Collector/Storage Solar Water Heaters. Solar Energy 75, 27-34

Smyth, M., Besheer, A., Zacharopoulos, A., Mondol, J., Pugsley, A., Novaes, M. (2015). Experimental evaluation of a Hybrid Photovoltaic/Solar Thermal (HyPV/T) Façade Module. Proceedings EURO ELECS Conference 21-23 July 2015, Guimarães, Portugal.

Smyth, M., Quinlan, P., Mondol, J., Zacharopoulos, A., McLarnon, D., Pugsley, A. (2018). The experimental evaluation and improvements of a novel thermal diode pre-heat solar water heater under simulated solar conditions. Renewable Energy 121, 116-122

Smyth, M., Pugsley, A., Hanna, G., Zacharopoulos, A., Besheer, A., Savvides, A. (2019). Experimental performance characterisation of a Hybrid Photovoltaic/Solar Thermal Façade module compared to a flat Integrated Collector Storage Solar Water Heater module. Renewable Energy 137 (2019) 137-143

Sorgato, M., Schneider, K., Rüther., R. (2018). Technical and economic evaluation of thin-film CdTe building-integrated photovoltaics (BIPV) replacing façade and rooftop materials in office buildings in a warm and sunny climate. Renewable Energy 118 (2018) 84-98

Stackhouse, P., Zhang, T., Westberg, D., Barnett, A., Bristow, T., Macpherson, B., Hoell, J. (2018). POWER Release 8.0.1 (with GIS Applications) Methodology, Data Parameters, Sources, & Validation. Data Version 8.0.1. Web Site Version 1.1.0. Hampton, USA: NASA LaRC, Langley Research Center.

Tripanagnostopoulos, Y., Souliotis M. and Nousia, T. (2000). Solar Collectors with Coloured Absorbers. Solar Energy 68 (4) 343-356

Yang, T., Athienitis, A. (2016). A review of research and developments of building-integrated photovoltaic/thermal (BIPV/T) systems. Renewable and Sustainable Energy Reviews 66 (2016) 886–912

Yao, J., Xu, H., Dai, Y., Huang, M. (2020). Performance analysis of solar assisted heat pump coupled with build-in PCM heat storage based on PV/T panel. Solar Energy 197 (2020) 279–291

Zacharopoulos, A., Mondol, J., Smyth, M., Hyde, T., O'Brien, V. (2009). State of the Art Solar Simulator with Flexible Mounting. Proceedings ISES Solar World Congress, 11-14 October 2009, Johannesburg, South Africa, pp 854-863

Zhou, J., Zhu, Z., Zhao, X., Yuan, Y., Myers, S. (2020). Theoretical and experimental study of a novel solar indirect expansion heat pump system employing mini channel PV/T and thermal panels. Renewable Energy AIP (doi.org/10.1016/j.renene.2019.11.054)

Ziapour, B., Palideh, V., Mohammadnia, A. (2014). Study of an improved integrated collector-storage solar water heater combined with the photovoltaic cells. Energy Conversion and Management 86 (2014) 587–594.

Zondag, H. (2008). Flat-plate PV–thermal collectors and systems: a review. Renewable & Sustainable Energy Reviews 12, 891–959.